

Article

# Thermodynamic Optimization of a Geothermal-Based Organic Rankine Cycle System Using an Artificial Bee Colony Algorithm

Osman Özkaraca <sup>1,\*</sup> , Pınar Keçebaş <sup>2</sup>, Cihan Demircan <sup>3</sup> and Ali Keçebaş <sup>4,\*</sup> 

<sup>1</sup> Department of Information Systems Engineering, Technology Faculty, Muğla Sıtkı Koçman University, 48000 Muğla, Turkey

<sup>2</sup> Department of Energy, Graduate School of Natural and Applied Sciences, Muğla Sıtkı Koçman University, 48000 Muğla, Turkey; pgkecebas@gmail.com

<sup>3</sup> Department of Energy Systems Engineering, Graduate School of Natural and Applied Sciences, Süleyman Demirel University, 32260 Isparta, Turkey; cihandemircan48@gmail.com

<sup>4</sup> Department of Energy Systems Engineering, Technology Faculty, Muğla Sıtkı Koçman University, 48000 Muğla, Turkey

\* Correspondence: osmanozkaraca@mu.edu.tr (O.Ö.); alikecebas@mu.edu.tr (A.K.);  
Tel.: +90-252-211-5526 (O.Ö.); +90-252-211-5471 (A.K.)

Received: 5 September 2017; Accepted: 20 October 2017; Published: 25 October 2017

**Abstract:** Geothermal energy is a renewable form of energy, however due to misuse, processing and management issues, it is necessary to use the resource more efficiently. To increase energy efficiency, energy systems engineers carry out careful energy control studies and offer alternative solutions. With this aim, this study was conducted to improve the performance of a real operating air-cooled organic Rankine cycle binary geothermal power plant (GPP) and its components in the aspects of thermodynamic modeling, exergy analysis and optimization processes. In-depth information is obtained about the exergy (maximum work a system can make), exergy losses and destruction at the power plant and its components. Thus the performance of the power plant may be predicted with reasonable accuracy and better understanding is gained for the physical process to be used in improving the performance of the power plant. The results of the exergy analysis show that total exergy production rate and exergy efficiency of the GPP are 21 MW and 14.52%, respectively, after removing parasitic loads. The highest amount of exergy destruction occurs, respectively, in condenser 2, vaporizer HH2, condenser 1, pumps 1 and 2 as components requiring priority performance improvement. To maximize the system exergy efficiency, the artificial bee colony (ABC) is applied to the model that simulates the actual GPP. Under all the optimization conditions, the maximum exergy efficiency for the GPP and its components is obtained. Two of these conditions such as Case 4 related to the turbine and Case 12 related to the condenser have the best performance. As a result, the ABC optimization method provides better quality information than exergy analysis. Based on the guidance of this study, the performance of power plants based on geothermal energy and other energy resources may be improved.

**Keywords:** geothermal power plant; Organic Rankine Cycle (ORC); thermodynamic modeling; exergy analysis; Artificial Bee Colony (ABC); performance improvement

## 1. Introduction

Geothermal energy is hot water, steam, gas or thermal energy within hot dry rocks that has accumulated under pressure at a variety of depths in the crust. In other words, geothermal energy may be defined as thermal energy of the globe [1]. It is estimated that the crust has 5.4 billion EJ of thermal energy. If just 0.1% of this energy could be used, world energy consumption needs for 10,000

years could be met. However, it is very difficult to use the Earth's energy at this scale and it requires advanced technology [2]. Geothermal energy is considered to be a clean, reliable and safe renewable energy resource [3]. Linked to the reservoir fluid temperature, geothermal resources are classified as low ( $<90\text{ }^{\circ}\text{C}$ ), moderate ( $90\text{ }^{\circ}\text{C}$ – $150\text{ }^{\circ}\text{C}$ ) and high ( $>150\text{ }^{\circ}\text{C}$ ) enthalpy resources [4]. Historically Conti created the first device producing electricity from a geothermal steam well in the town of Lardello in Italy in 1904 and in 1913 the first commercial geothermal energy system was linked to the grid with a 250 kW alternator in the same place [5]. The success of these experiments led to small scale electricity production from geothermal resources in the city of Beppu in Japan in 1919 and from geysers in California in 1921. New Zealand's Wairakei station began operations in 1958, which was a turning point in the technological history of electricity production and it was the first facility to use wet steam technology (flash steam). Previous power plants were limited to the use of geothermal reservoirs containing dry steam [6]. In 1977 the first dual flash power plant began operating in Japan and in 1984 geothermal energy power plants using binary cycles started to operate [7]. Thus electricity production from geothermal energy spread around the world and over one hundred years have passed since the first day electricity was produced from geothermal resources to the present. In this respect, Turkey has a long history of electricity production from this type of energy. In 1984 Turkey's first geothermal energy power plant with 20.4 MW<sub>e</sub> installed power was opened in Denizli (Kızıldere) [8]. However, to date its share within the variety of energy resources used in Turkey has not reached desired levels. Instead, the basic use of Turkey's geothermal energy is direct usage [9].

Geothermal power plants use hydrothermal resources with hydro and thermal components. Hot water or steam turns a turbine and is used to generate electricity. Geothermal power plants require hydrothermal resources with high temperatures (nearly  $150\text{ }^{\circ}\text{C}$ – $370\text{ }^{\circ}\text{C}$ ) coming from hot water wells or dry steam wells [10]. In this situation, for electricity production from geothermal resources to be possible, generally a minimum temperature of  $150\text{ }^{\circ}\text{C}$  is required. The mean temperature gradient within the earth's crust is  $25\text{ }^{\circ}\text{C}/\text{km}$ – $30\text{ }^{\circ}\text{C}/\text{km}$ . As a result, for electricity production from geothermal, either a deep temperature drilling is required or regions with high temperature gradient should be chosen [11]. Nearly all geothermal power plants can be divided into four categories: dry steam, single flash, dual flash and binary designs. Power plant design is generally a function of the temperature and pressure of the available geothermal resource.

As mentioned above, it is known that for electricity production in power plants, fluid temperatures above  $150\text{ }^{\circ}\text{C}$  must be ensured. Additionally, electricity generation from binary geothermal power plants may use very low temperatures. In situations where the temperature of geothermal fluid coming from the production well is below  $150\text{ }^{\circ}\text{C}$  (typically between  $110\text{ }^{\circ}\text{C}$  and  $180\text{ }^{\circ}\text{C}$ ), it is not possible to evaporate the fluid flow to form steam. Therefore, binary geothermal power plants are typically used for these applications. A basic binary geothermal power plant operates a geothermal fluid (brine) to ensure thermal input of a pressurized fluid (organic fluid) into an Organic Rankine Cycle (ORC). Geothermal brine heats the organic working fluid (R134a, *n*-pentane, isopentane) in a preheater and evaporator which later vaporizes. This steam produces electrical energy by passing through a turbine driving the generator. The working fluid passing through the turbine is generally condensed in an air-cooled condenser before being pumped to the preheater [12].

After the oil crisis of the 1970s, it was understood that energy efficiency alone could not determine how properly energy was used. Thus exergy analyses began to gain great importance. However, the basis of exergy extends to the 1870s. It was first proposed by Gibbs in 1878 [13]. The exergy concept as a word was first used by Rant in the year 1953 [4]. Available energy [14], available work [13] and availability or maximum beneficial work [15] concepts were proposed with equivalent meaning to exergy. İleri and Gürer [16] brought energy use, in addition to exergy use, to the agenda in Turkey in 1995. The results of their studies completed exergy analysis of apparently efficient systems, and revealed just how inefficient these systems actually were.

The most appropriate design for geothermal power plants is a complicated work encompassing multiple scientific and engineering disciplines. As a result, information should be synthesized about

a variety of topics to make appropriate decisions related to the approach to be used and research methods [17–22]. Currently characterization of energy resources, power plant design and engineering optimization topics require creation of a conceptual framework comprising the knowledge of the latest available technology and current research. Consequently, energy inputs to the electricity power plant requiring knowledge related to available geothermal resources in the world, in general, should be accurately estimated. During the process of geothermal power plant design, design and modelling research should be fully understood, requiring detailed investigation of operating and continuing power plants. Also, conscious and correct decisions should be made relating to application of the most appropriate optimization techniques. This requires detailed investigation of the literature emphasizing techniques to bring energy power plants or thermal systems to the best state and optimization methods for engineering applications. The majority of scientific studies have focused on design optimization, selection of appropriate fluid, exergy/energy analyses and a variety of techno-economic research. Additionally, a common characteristic of ORC-based systems is the multiple nature of working conditions. The majority of application areas experience variations in thermal resource (or cooling processes) over time and the system should adapt to the working regime to ensure optimum performance. There are few studies related to control aspects and off-design performance of ORC systems [23–35]. Thus, all the following studies are related to low temperature ORCs.

As the development of renewable energy resources has intensified, the researches into ORC technologies producing electricity from low enthalpy geothermal resources have increased. The majority of these studies revolve around geothermal binary power plants and their design. At the beginning of the 1970s, Anderson [36] explained the design of the first binary geothermal binary power plant in the USA, known as Magmamax (and second globally). A short while after, Bliem et al. [37] developed a computer model to research the effect on levelized cost of electricity (LCOE) with five different temperatures for a Rankine cycle power plant with simple propane-based geothermal resource. Kanoğlu [38] studied the design of a Rankine cycle power plant with dual pressure using isopentane as working fluid. This research showed that developing efficiency of turbine and condenser provided the largest improvement to power plant efficiency. It also proved that in air-cooled power plants seasonally changing condenser temperatures caused significant changes in power plant output. Öztürk et al. [39] investigated the energy and exergy analysis for the Kızıldere geothermal power plant. This plant was the first geothermal power plant built in Turkey in 1974. They used real power plant data and researched the effect of a variety of dead situation characteristics on Kızıldere geothermal power plant exergy efficiency to find the optimum performance and working conditions. The calculations given are based on a mean pressure of 0.095 MPa and mean reference temperature of 16 °C. The energy and exergy efficiencies for the whole power plant were determined as 4.9% and 20.5% respectively. Hettiarachchi et al. [40] applied a more sophisticated optimization method (steepest descent) to design a simple water-cooled ORC binary energy power plant. This study varied the speed of geothermal fluid and cooling water for a variety of working fluids in addition to the evaporation and condensation temperature to minimize the net power output rate of the heat exchanger area. The results of this optimization showed that choice of working fluid may have a significant effect on power plant costs. Sohel et al. [41] presented optimization of an ORC geothermal power plant performance by optimizing study point parameters based on real time hourly weather data and geothermal fluid flow rates in the search for performance improvement. They characterized the Rotokawa geothermal power plant using energy generation performance and local weather conditions. On the hottest day, the maximum production increase was 6.8%. Due to the operating binary unit production capacity of the Rotokawa power plant with 35 MW, investment in a water-enriched air-cooled system would provide 2 MW productions on the hottest days. Franco and Villani [42] used an iterative optimization approach and produced a comprehensive data set related to design of geothermal binary power plants. In this study they developed a method to identify optimum combinations of working fluid and cycle type for three different geothermal input and re-injection temperature sets. The method explained by Franco and Villani [42] considered supercritical

cycles, dual pressure Rankine cycles and classic Rankine cycles, in addition to hydrocarbons, synthetic cooling fluids and mixtures to discuss six different working fluids. The results of the study found different combinations of cycle type and working fluid were appropriate for different geothermal brine input and re-injection temperatures and the optimized solution produced significant improved exergetic efficiency. Sohel et al. [43] presented an iterative method to model the effect of environmental temperature on an air-cooled ORC. Environmental temperature affected the performance of condensers on both routes and so the performance of the whole cycle. Firstly, changing the balance pressure within the condenser changed the turbine output pressure and turbine pressure ratios. The turbine pressure ratio is an important parameter to determine energy produced by the turbine because it directly affects power plant output. Secondly changing the condenser output temperature and environmental temperature changes the pump input and output conditions. Thus the balance temperature and pressure in the vaporizer is affected. The developed method aimed to rebalance conditions for both the condenser and vaporizer. To show the validity of the method, they studied two situations based on performance of a real power plant. The developed method was stable and converged independently from the initial conditions permitted by the physical properties of the working fluid. This method is effective with appropriate initial conditions and limitations under static or dynamic variables for cycles using saturated steam in addition to over-heated steam. Ghasemi et al. [44] developed a model for an operating ORC using low temperature geothermal resources. Equipped with an air-cooled condenser system, they used Aspen Plus to simulate the performance of the present ORC. The model included real properties of all components and was confirmed by 5000 measurements over a broad interval of environmental temperature. Thus the net output power of the system appeared to be maximized. Different optimal operating strategies were recommended linked to environmental temperature. As the environmental temperature increased in the study, optimum heating values increased and they stated a 9% increase was ensured in total power produced each year. Their study used a representative hourly environmental temperature profile to determine the most appropriate power station design for a certain climate.

In the recent literature, there are not so many models based on physical understanding, broad conceptual design and optimization modelling to estimate the performance of binary geothermal ORC power plant. Generally, it has been focused on the power output and system performance (thermodynamic, economic and environmental) of low temperature sourced power plants, especially efficiency as objective functions, geothermal brine reservoir or crustal output properties, environmental temperature, working fluid selection for ORC, evaluation of new analysis methods, new cycle designs, adding/removing components to existing cycles or renovation studies. However, considering the geothermal power plants and their performance analyses, it will be beneficial to rapidly produce a simple thermodynamic model simulating the working cycle. Especially the use of the ABC optimization method used for modelling thermal systems will determine improvement potentials of system components, interactions between components and aspects and potentials for energy saving to provide better performance of real system models. To the best of the authors' knowledge, this topic is examined for the first time in the literature. This has formed the source of motivation for the authors.

## 2. Modelling, Analysis and Optimization of a System

From a geothermal perspective, the geothermal well is the heart of a geothermal power plant. The enthalpy and mass flow of the produced geofluid determine how the system will be chosen. The characteristics of the wellbore and therefore geofluid change from field to field and, in some cases, from well to well. This leads to the examination of each system separately. Thus, this study to characterize system performance is completed in three steps. The first step is to apply exergy analysis to a real operating geothermal power plant. In the second step, a thermodynamic model simulating the system and/or system components is developed. As a final step, the developed model is optimized with the artificial bee colony (ABC) method for the objective function of maximizing the system exergy efficiency.

### 2.1. Description of the Sinem GPP as a Case Study

Turkey's geothermal fields have a wide regional distribution linked to tectonic and volcanic activity. In this situation, the majority of high enthalpy or high temperature geothermal fields are compressed in the continental rift zones of the Menderes Massif and are due to later expanding tectonic activity. As a result, these high temperature geothermal fields are found within the continental rift belt of the Büyük Menderes basin. One of these fields is the Hıdırbeyli region of Germencik county in Aydın province/Turkey with five geothermal power plants (GPP) operating under the names İrem GPP (20 MW), Sinem GPP (24 MW), Deniz GPP (24 MW), Kerem GPP (24 MW) and Ken 1 GPP (24 MW) belonging to the Maren Maras Electricity Generation Inc. with 116 MW capacity [45]. In this study it is chosen the Sinem GPP operating at 24 MW installed power within this geothermal field. The schematic flow diagram for Sinem GPP is given in Figure 1.

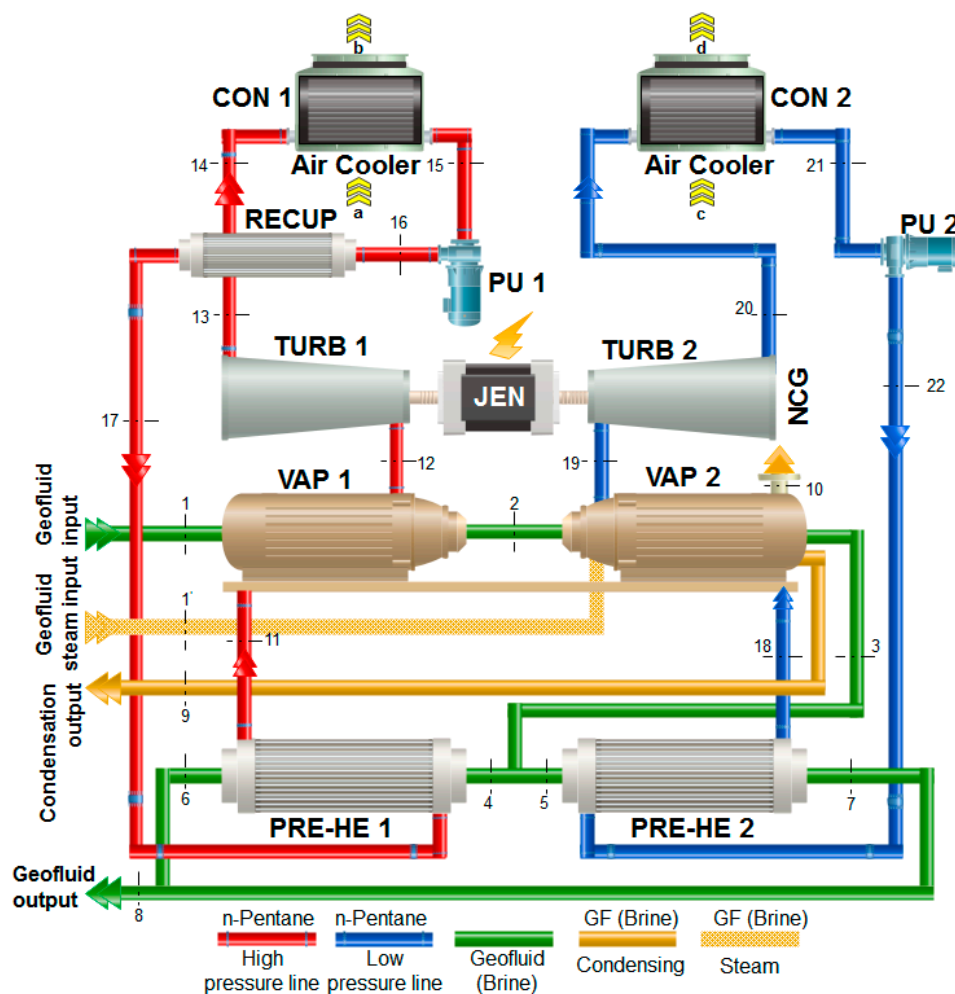


**Figure 1.** A schematic flow diagram of the Sinem GPP.

This GPP works in accordance with an air-cooled geothermal binary organic Rankine cycle. It started operating in July 2012. From Figure 1, the Sinem GPP with the air-cooled binary organic Rankine cycle comprises evaporators (VAP 1, VAP 2, PREHE 1, PREHE 2 and RECUP), turbines (TURB 1 and TURB 2), generator (GEN), condensers (CON 1 and CON 2), fans (FAN 1 and FAN 2) and pumps (PU 1 and PU 2) components at level I and II. The heat input rate at the GPP system currently obtains mixed geothermal fluids from 3 artesian production wells (GM3, GM5 and GM8), with each well-head installed with a vertical separator to divide two phase fluid into geofluid (liquid brine) and saturated steam. These production wells have temperatures of 165 °C–170 °C, pressure of 10 bar–14 bar and flow rate of 1100 ton/h–1500 ton/h.

Initially high pressure steam with 165 °C temperature, 8.33 kg/s flow and 1040 kPa is obtained from the separators. This steam comprises 30% non-condensable gases (NCG). The remaining 70% is geothermal fluid steam. Then geofluid with 165 °C, 1040 kPa and 445 kg/s is obtained from separators. Only the power plant of Sinem GPP is only examined as it can be seen from Figure 1. The production wells, separators, automation/safety systems, re-injection wells, piping and fittings of the GPP are outside the scope of the study. Steam and liquid geofluids are prepared with the properties mentioned above reach the power plant. Thus, the binary organic Rankine cycle of the GPP begins the operation. The binary ORC comprises two different classic Rankine cycles alongside and separates each other.

The Sinem GPP, like all these systems, is operated in accordance with the T-s flow diagrams as illustrated in Figure 2. The temperatures, pressures, mass flow rates of the system are listed in Table 1, based on the thermodynamic states indicated in Figure 1, for the chosen day. As can be seen in Figure 2 and Table 1, the cycles are called as level I with 160 kg/s flow rate (high pressure of 1261 kPa) and level II with 196 kg/s flow rate (low pressure of 687 kPa). As follows from Figure 1 and Table 1, the geofluid first compresses the vaporizer VAP 1 on level I heating *n*-pentane as working fluid of the ORC. Later the geofluid passes to the vaporizer VAP 2 on level II and heats *n*-pentane. As the geofluid in VAP 2 on level II has low temperature and pressure, the stream of geofluid obtained from the separators is inputted here. Both the geofluid and steam pass through VAP 2 without mixing. In the output from VAP 2, the NCG and steam is released to the atmosphere, and the condensed geofluid is compressed for re-injection. The geofluid emerges from VAP 2. Here it passes through the pre-heaters PREHE 1 and PREHE 2 simultaneously. However, for safety reasons, the pre-heaters are taken offline when a certain temperature is reached. The geofluid (85 °C and 590 kPa) collected at the output of the preheaters is pumped to the re-injection wells (GM4 and GM14) together with the condensed geofluid.

**Table 1.** Thermodynamic properties collected and exergy rate calculated for each line number in real operating conditions of the Sinem GPP (on 14 April 2013).

Line, j	Fluid Type	Temperature $T_j$ (°C)	Pressure $P_j$ (kPa)	Mass Flow Rate $m_j$ (kg/s)	Exergy Rate $Ex_j$ (kW)
1	Geofluid	164	1040	445	52,693
1'	Geofluid–steam	165	1040	5.83	699
1'	NCG	165	1040	2.50	380
2	Geofluid	136	730	445	36,010
3	Geofluid	110	690	445	22,589
4	Geofluid	110	690	22.250	11,295
5	Geofluid	110	690	222.50	11,295
6	Geofluid	89	590	222.50	7021
7	Geofluid	81	570	222.50	5616
8	Geofluid	85	590	445	12,447
9	Geofluid	107	690	0.83	40
10'	Geofluid–steam	107	690	5.25	253
10'	NCG	107	690	2.25	257
11	<i>n</i> -pentane	105	1261	160	4776
12	<i>n</i> -pentane	137.4	1261	160	20,142
13	<i>n</i> -pentane	82	150	160	7237
14	<i>n</i> -pentane	60	150	160	6193
15	<i>n</i> -pentane	31	150	160	123
16	<i>n</i> -pentane	37	1261	160	520
17	<i>n</i> -pentane	55	1261	160	1141
18	<i>n</i> -pentane	106	687	169	5018
19	<i>n</i> -pentane	109	687	169	16,512
20	<i>n</i> -pentane	69	119	169	5713
21	<i>n</i> -pentane	33	119	169	157
22	<i>n</i> -pentane	39	687	169	431
a	Air	18	101	2000	0
b	Air	19	106	2000	8048
c	Air	18	101	2000	0
d	Air	19	106	2000	8048

As seen in Figure 2a and Table 1, the *n*-pentane heated in VAP 1 on level I is sent to turbine TURB 1 with 137.4 °C and 1261 kPa pressure as superheated steam (at point 12), to rotate the turbine.

The *n*-pentane with 82 °C and 150 kPa emerging from TURB 1 is then sent to the recuperator RECUP (at point 13). If the *n*-pentane emerging from the turbine still carries high energy, this high energy is stored in RECUP and later is used to transfer to *n*-pentane coming from the pump PU 1. The *n*-pentane coming from RECUP enters the air-cooled condenser CON 1 at lower temperature of 60 °C (at point 14). The air-cooled condenser CON 1 lowers the temperature of the *n*-pentane to 31 °C and 150 kPa (at point 15) to produce liquid, and this passes to pump PU 1. The *n*-pentane is pumped at 1261 kPa pressure from PU 1 to the recuperator RECUP (at point 16) and regains the previously stored heat in RECUP to increase the temperature. Thus the efficiency of the heat exchangers PREHE 1 and VAP 1 acting as evaporators is increased. The *n*-pentane heated by RECUP is sent to the pre-heater PREHE 1 (at point 17) and from there to the vaporizer VAP 1 again (at point 11). Thus the organic Rankine cycle returns to the start and this continues repeatedly. To increase the efficiency of the GPP, this works in coordination with another ORC (level II). As shown in Figure 2b and Table 1, the *n*-pentane heated in VAP 2 on level II has 109 °C and 687 kPa pressure (at point 19) and is sent to rotate the turbine TURB 2 as superheated steam. Later, different to level I, the *n*-pentane is sent to the air-cooled condenser CON 2 at 69 °C temperature (at point 20). From the air-cooled condenser CON 2, the *n*-pentane is sent to the pump PU 2 at 33 °C and 119 kPa (at point 21) as liquid. In pump PU 2, the *n*-pentane pressure has risen to 687 kPa and is pumped to pre-heater PREHE 2 (at point 22). Passing through PREHE 2 and later VAP 2 (at point 18), the cycle on level II is completed. In conclusion, the power generated by rotating the turbines TURB 1 and TURB 2 produces electricity in the generator GEN (see Figure 1). This part consists of two turbines on the same shaft with *n*-pentane flowing in opposite directions. Before turbines, the pentane, supplied in sufficient pressure, is sent to the turbines by opening the injection valves. It is preferred because of its lower capital cost and the balance on the thrust loads. Injection valves on turbines are used to rotate the shaft at 3000 rpm in electricity generation. Of the 21 MW obtained from the turbines, nearly 6.79 MW is used by equipment installed in the power plant. The rest of generated energy is transmitted to Germencik switchyard and to the interconnected power lines.

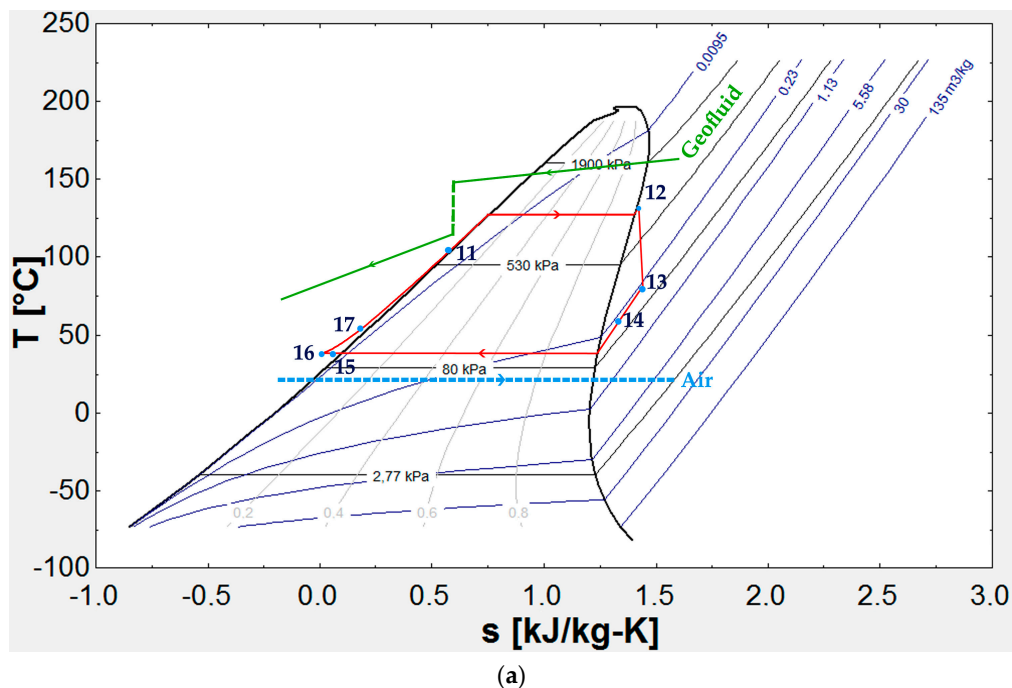
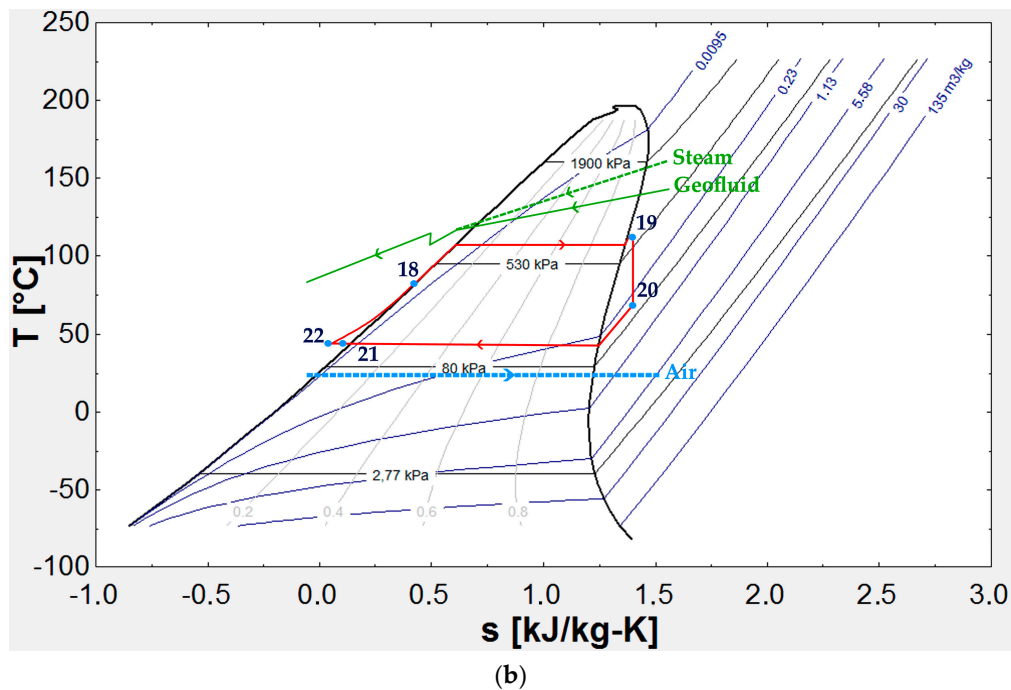


Figure 2. Cont.



**Figure 2.** T-s diagrams for the (a) level I and (b) level II in the running of the real geothermal binary ORC power plant (Sinem GPP) (*n*-pentane for ORC in red, geofluid in green and air in blue).

## 2.2. Thermodynamic Analysis

It is well known that the three balance equations namely mass, energy and exergy balance equations are used to find the heat input, the rate of exergy decrease, the rate of irreversibility, and the energy and exergy efficiencies for a general steady-state, steady-flow process.

In general, the mass balance equation can be expressed in the rate form as:

$$\sum \dot{m}_{in} = \sum \dot{m}_{out} \quad (1)$$

where  $\dot{m}$  is the mass flow rate, and the subscript “in” stands for inlet and “out” for outlet.

The general energy balance can be expressed by all energy terms as follows as below where the changes in kinetic and potential energy are neglected:

$$\dot{Q} + \sum \dot{m}_{in} h_{in} = \dot{W} + \sum \dot{m}_{out} h_{out} \quad (2)$$

where  $\dot{Q} = \dot{Q}_{net,in} = \dot{Q}_{in} - \dot{Q}_{out}$  is the rate of net heat input,  $\dot{W} = \dot{W}_{net,out} = \dot{W}_{out} - \dot{W}_{in}$  is the rate of net work output, and  $h$  is the specific enthalpy.

Assuming no changes in kinetic and potential energies with no heat or work transfers, the energy balance given in Equation (2) can be simplified to flow enthalpies only:

$$\sum \dot{m}_{in} h_{in} = \sum \dot{m}_{out} h_{out} \quad (3)$$

Exergy analysis shows the locations and causes of inefficiency and losses in an energy conversion system. Exergy analysis of a system creates a general equation for the whole system and balance equations representing the balance component level of a system. Thus for a system the general exergy rate balance can be expressed as [46]:

$$\dot{E}_{X,F,tot} = \dot{E}_{X,P,tot} + \sum_k \dot{E}_{X,D,k} + \dot{E}_{X,L,tot} \quad (4)$$

and more explicitly:

$$\sum \left(1 - \frac{T_0}{T_k}\right) \dot{Q}_k - \dot{W} + \sum \dot{m}_{in} \psi_{in} - \sum \dot{m}_{out} \psi_{out} = \dot{E}x_D \quad (5)$$

where  $\dot{E}x_F$ ,  $\dot{E}x_P$ ,  $\dot{E}x_D$  and  $\dot{E}x_L$  are the exergy rates associated with the fuel, product, exergy destruction and exergy loss of the overall system, respectively. In addition,  $\dot{Q}_k$  is the heat transfer rate crossing the boundary at temperature  $T_k$  at location  $k$ ,  $\dot{W}$  is the work rate,  $\psi$  is the flow exergy, and the subscript zero indicates properties at the restricted dead state of  $P_0$  and  $T_0$ . Their values are taken as 18 °C and 1 bar in the dead state.

The unit exergy rate is expressed by:

$$\dot{E}x_j = \dot{m}_j \psi_j \quad (6)$$

where  $\dot{E}x_j$  is the unit exergy rate of the  $j$ th location in kW and  $\psi_j$  is the specific flow exergy in kJ/kg as follows:

$$\psi = (h - h_0) - T_0(s - s_0) \quad (7)$$

where  $h_0$ ,  $T_0$  and  $s_0$  denote the enthalpy (in kJ/kg K), temperature (in °C or K) and entropy (in kJ/kg K) in the reference case, respectively.

For exergy destruction (or irreversibility), the entropy generation  $\dot{S}_{gen}$  is calculated first and used in the following equation:

$$\dot{I}_k = \dot{E}x_{D,k} = T_0 \dot{S}_{gen} \quad (8)$$

To assess exergy analysis, the exergy efficiency valid for the system and its components may be defined as follows:

$$\varepsilon_{system} = \frac{\dot{E}x_{output}}{\dot{E}x_{input}} \quad (9)$$

where “output” refers to “net output” or “product” or “desired value”, and “input” refers to “given” or “used”.

### 2.3. Modelling of the System

For the real operational Sinem GPP, some control volumes are identified and thermodynamic balance equations are applied to these control volumes. These control volumes are the vaporizers (VAP 1 and VAP 2) and pre-heaters (PREHE 1 and PREHE 2) allowing heat exchange between the geofluid and  $n$ -pentane as working fluid, condensers (CON 1 and CON 2) allowing heat exchange between the air and  $n$ -pentane, and the recuperator (RECUP) using only  $n$ -pentane, turbines (TURB 1 and TURB 2), pumps (PU 1 and PU 2) and fans (FAN 1 and FAN 2), as seen in Figure 1. The basic aim of the model is to research the interactions between the components mentioned above on performance of the whole system, the potentials to improvement and energy saving aspects and potentials. Additionally, some parametric studies are completed to investigate the effect of some important parameters on the performance of the air-cooled binary geothermal ORC (see Figure 2).

The thermodynamic properties of the pure water for geofluid (brine),  $n$ -pentane as working fluid and air as an ideal gas in each control volume is determined from the COOLPROP software [47,48]. The MATLAB software [49] is used for thermodynamic balance equations and numerical calculations. In this way, the thermodynamic fluid properties in COOLPROP may be included in MATLAB software (2015b, MathWorks, Natick, MA, USA). Shortly, an algorithm is used for thermodynamic analysis and modelling of Sinem GPP in the MATLAB software. For simplicity, the balance equations for the algorithm models are not given in the text; however they are given in Appendix A Tables A1 and A2. The basic assumptions of the integrated model system in exergy analysis are as follows:

- System and its components work in stable state and stable volume conditions,
- Kinetic and potential losses are ignored,
- Heat losses from components are collected in a single location,
- Pressure drops in evaporators, condensers, valves and pipes are collected in a single location,
- For geofluid (brine), the thermodynamic properties of water are used. By doing so, any possible effects of salts and incondensable gases that might be present in the geofluid are neglected [50].
- The pressure losses due to the liquid flow friction were considered negligible.
- In air-cooled condensers, air is accepted as an ideal gas with homogenous distribution,
- Isentropic efficiencies of turbines, pumps and fans are only fixed for the optimization process.

In order to build a model that will simulate the Sinem GPP completely, an algorithm working in accordance with the T-s flow diagram in Figure 2 using the real data in Table 1 is designed. The algorithm is modelled with a construct created between components using data collected from the real system. This construct is presented in Figure 3. During modelling, for each piece of components on the T-s flow diagrams (Figure 2), values of parameters, effectiveness coefficient ( $\tilde{\epsilon}_k$ ) and isentropic efficiency ( $\eta_k$ ), are changed and attempts are made to bring the model output parameters (temperature and pressure) closest to or to the same value as the operation parameters (temperature and pressures) (in Table 1) collected from the Sinem GPP. Thus, the developed model will imitate the real GPP system. As can be seen in Figure 3 and Appendix A Table A2,  $\tilde{\epsilon}_k$  and  $\eta_k$  are effectiveness coefficient associated with  $\epsilon$ -NTU method for heat exchangers (vaporizers, condensers, pre-heaters and recuperator) and isentropic efficiency for turbines and pumps, respectively. These are clearly defined as the parameters used to try to make the model match the operational state of the GPP. Their constants used to match the real system to the model are within the boundaries defined by the equipment manufacturer. Their values are 0.82 and 0.88 for VAPs, 0.92 and 0.95 for PREHEs, 0.49 for RECUP, 0.68 and 0.75 for CONs, 0.92 and 0.81 for TURBs, 0.96 and 0.97 for PUs, respectively.

For the optimization process, the  $\tilde{\epsilon}_k$  and  $\eta_k$  values of the real operating GPP are fixed and then data given in Table 1 for all line numbers in the system shown in Figure 1 are optimized to maximize the system exergy efficiency. The Artificial Bee Colony (ABC) algorithm is used for optimization of Sinem GPP. The objective function is accepted as the system exergy efficiency.

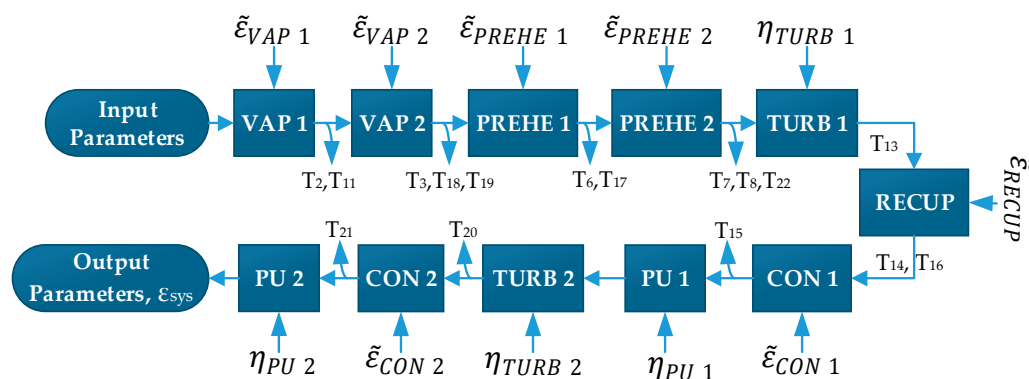


Figure 3. Flow diagram of the construct used for the most appropriate model of the Sinem GPP.

#### 2.4. Optimization: Artificial Bee Colony

Investigation of processes involving intelligent behaviour present in nature has led researchers to develop new optimization methods. Karaboğa [51] developed the Artificial Bee Colony (ABC) algorithm by modelling the behaviour of bees searching for food. The basis of the ABC algorithm includes some assumptions for simplicity. The first of these is the nectar from each source can only be obtained by one worker bee. In other words, the number of duty bees is equal to the number of food sources. The number of worker bees is accepted as equal to the number of observer bees. The worker

bee assigned to a source with nectar fully consumed transforms into an explorer bee. Possible solutions of optimization problems for locations of food sources and nectar amounts of the sources are equivalent to the quality (fit) of the solutions related to those sources. Consequently, the ABC algorithm attempts to locate the source with most nectar and attempts to find a problem's minimum or maximum point within solution space. The process steps belonging to this model are given below [52–55]:

- At the start of the food search process, explorer bees randomly search the environment and begin to search for food.
- After food sources have been found, explorer bees become worker bees and begin to carry the nectar found at the source into the hive. Each worker bee empties the nectar on return to the hive and at this point either returns to the food source or communicates information related to the food source with the observer bees waiting in the hive through dance displayed in the dance area. If the food source is consumed, the duty bee transforms into an explorer bee and begins to search for new food sources.
- Observer bees waiting in the hive watch dances indicating rich food sources and choose a food source linked to the dance frequency which is proportional to the food quality.

For initial production of food source areas, if we think of the food sources surrounding the hive as search space, the algorithm is based on randomly producing food sources equivalent to solutions in search space. The random location production process is completed by producing random values between the upper and lower limits for each parameter as seen in [54,55]:

$$x_{ij} = x_j^{\min} + \text{rad}(0,1) \left( x_j^{\max} - x_j^{\min} \right) \begin{cases} i = 1, \dots, SN \\ j = 1, \dots, D \end{cases} \quad (10)$$

where SN is the number of food sources and D represents the number of parameters to be optimized.

After the initial stage, the worker bee, observer bee and explorer bee process for food sources begin, with an attempt made to find better sources. For stopping criteria of the ABC algorithm, the maximum cycle number (MCN), acceptable error value or other stopping criteria can be used. During this optimization process, the number of worker bees is equal to the number of food sources. Worker bees attempt to determine new food sources near food sources and assess their quality. If the new food source is better, it is remembered. To determine neighbouring food sources to the new source, the simulation is given in:

$$v_{ij} = x_{ij} + \varphi_{ij} \left( x_{ij} - x_{kj} \right) \quad (11)$$

where, as the difference between the random values  $x_{ij}$  and  $x_{kj}$  reduces, in other words as the solutions equivalents, the variation amount in the  $x_{ij}$  parameter reduces. Thus, as the regional optimal solution is approached, the variation amount adaptively decreases. The  $v_i$  parameter produced within the limits represents a new source and its quality is assigned by calculating the fit value as given below:

$$\text{fitness}_i \begin{cases} \frac{1}{1+f_i}, & f_i \geq 0 \\ 1 + |f_i|, & f_i < 0 \end{cases} \quad (12)$$

where  $f_i$  is the cost values of the solution of the  $v_i$  source. Depending on the nectar amounts between  $x_i$  and  $v_i$ , in other words the fit, a greedy selection process is applied. If the newly found  $v_i$  solution is better, the location of the old food source is wiped from the duty bee's memory and the location of  $v_i$  source is noted. Otherwise, the worker bee continues going to  $x_i$  source and as the  $x_i$  solution was not developed the failure counter ( $\text{failure}_i$ ) for this source increases by one; if it succeeds the counter resets to zero.

After all worker bees have completed one cycle of research, they return to the hive and transmit information about nectar amounts of sources to observer bees. An observer bee uses the information transmitted by the dance to choose a region (source) in accordance with the nectar amount of the food

source. This is an example of the ABC algorithm displaying multiple interactions. The probabilistic selection process is made by using the fit values equivalent to the nectar amounts in the algorithm. The basis of the selection process linked to fit value in the ABC algorithm is completed using a roulette wheel. The angle of each section of the wheel is proportional to the fit value. That is, the fit value of a food source as a proportion to the total fit value of all sources expresses the relative selection probability for that source compared to other sources:

$$P_i = \frac{\text{fitness}_i}{\sum_{j=1}^{SN} \text{fitness}_j} \quad (13)$$

According to the probability calculation process, as the amount of nectar in a source increases (as the degree of fit increases), the number of observer bees selecting this region will increase. This characteristic shows that the ABC displays similar behaviour to the positive feedback characteristics revealed by natural bee behaviour. After the probability values of the algorithm are calculated, these values are used to produce a random number in the [0, 1] interval for each source in the selection process according to roulette wheel. If the  $p_i$  value is larger than this produced number, worker bees use Equation (11) like observer bees and produce a new solution for this source region. The new solution is assessed and the quality is calculated. Later the fit of the new solution is compared with the old solution and the better one is chosen by using the greedy selection process. If the new solution is better, this solution is replaced by the old solution and the failure counter is set to zero. Conversely, if the fit of the old solution is better, this solution is retained and the failure counter increases by one. This process continues until all observer bees are assigned to a food source region.

At the end of a cycle, all worker bees and observer bees have completed search processes and the solution failure counters are checked. Whether a bee benefitted from a source or not, in other words whether the nectar at that point has been consumed or not, is known from the solution failure counter. If the solution failure counter of a source is above a certain threshold value, the duty bee for that source should have left that consumed solution and started to search for another one. This means that the worker bee for a consumed source should become an explorer bee. The threshold value used to determine whether a source is consumed is an important control parameter for the ABC algorithm and is called the “limit”. For each cycle of a basic ABC algorithm, only one explorer bee is allowed out.

### 3. Results

In this study, an air-cooled binary geothermal organic Rankine cycle (ORC) power plant is thermodynamically modelled to observe, test and check its thermodynamic performance more accurately and rapidly. Additionally, to increase the modelled system performance, the artificial bee colony (ABC) method is used to maximize system exergy efficiency. With this aim, real operating data (flow rate, pressure and temperature values from input and output lines of system components) from an existing power plant were collected by the system’s Supervisory Control and Data Acquisition (SCADA) program on 14 April 2013. This date is a transitional period between winter and summer seasons for data from the Sinem GPP. The environmental temperature and pressure on that date were recorded as 18 °C and 1 bar, respectively. Later the operational data according to state numbers of Figure 1 are presented in Table 1 and the equations given in the Thermodynamic Analysis section are used to complete exergy analysis. The results of the exergy analysis for the real GPP are shown as the Grossman flow diagram in Figure 4. The exergy efficiency of the power plant is calculated as 39.1% based on the exergy input of geofluid (brine) and its steam entering the system. However, the power consumed in the operation of turbines, pumps, fans, auxiliary equipment of the GPP is met by the gross power generated by the plant. When this was deduced, the system exergy efficiency was found to be 14.52%. Turning to Figure 4, the result is that 60.9% of the exergy input rate entering the system is lost as waste heat (exergy loss and destruction). Of the exergy input rate of the geofluid entering the system, 23.7% and 0.5% is lost in the re-injection phase and in the phase of releasing NCG

into the atmosphere as exergy loss (heat loss-waste heat), respectively. Of the remaining exergy input rate, 20.6% and 15.6% are consumed as exergy destruction on levels I and II, respectively. The highest exergy destruction percentages for components are 4.6% from condenser CON 2 and vaporizer VAP 2, 3.7% from condenser CON 1 and then 3.6% from pumps and separators on level I and II.

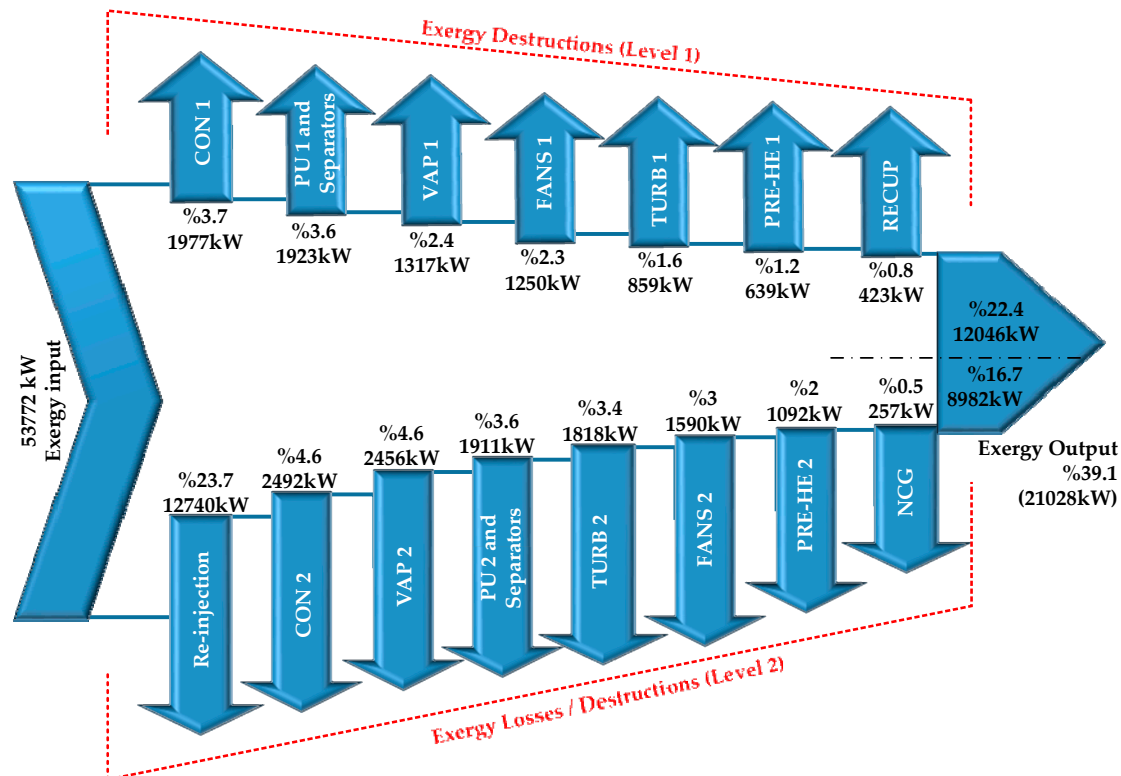
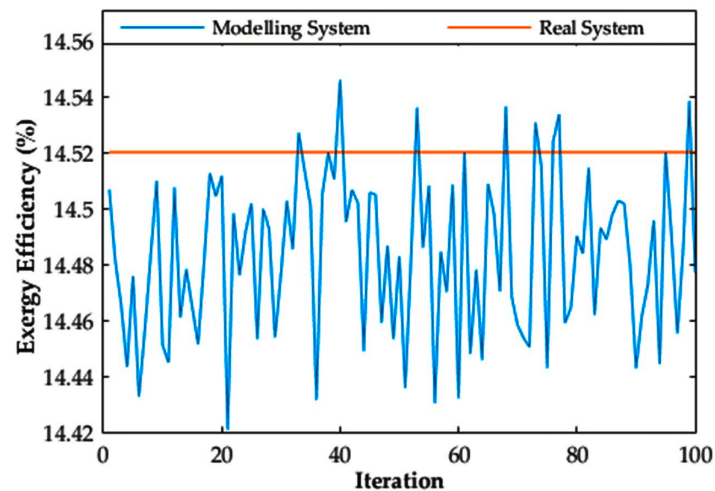


Figure 4. Grossman flow diagram for the exergy analysis results of the Sinem GPP.

As observed in Figure 4, there is approximately 53,772 kW exergy input rate into the system from the geofluid and its steam. Of this total exergy input rate, 12,740 kW is calculated as the exergy rate spent on re-injection, 11,102 kW is exergy destruction rate occurring in system components on level I, 8388 kW is exergy destruction rate of those in level II and 275 kW is the exergy loss rate from NCG. The highest exergy destruction rate in the GPP occurs in the condenser CON 2 in level II of the binary cycle. This is followed by VAP 2 on level II and then CON 1 on level I. In this situation the priority components requiring improvement are CON 2, VAP 2 and CON 1.

As described in the Modelling of the System section, modelling is based on the exergy analysis of a real GPP. The data (mass flow rate, temperature and pressure on steam lines in Figure 1) entering and exiting the system and its components are recorded momentarily. Thus, all the data are dynamic over time.

Two parameters ( $\tilde{\epsilon}_k$  and  $\eta_k$ ) with these data are established a relationship between the system components, so an integrated system model has been created. As a result, the behaviour of the model is very close to that of the real system and simulates it accurately. Therefore, the convergence behaviour of the model for modelling the real system according to the exergy efficiency is presented in Figure 5. Note that the exergy efficiency of the real system is 14.52%. It can be seen that the exergy efficiency of the model fluctuates with an increase in iteration number and varies between 14.42% and 14.55%. This fluctuation occurs during the matching process between the real system and the model. Regarding Figure 5, the maximum and minimum efficiencies equal respectively the 40th and 21th iterations number occurring at exergy efficiency of the model and the efficiency of the real system is very close to that of the model.



**Figure 5.** The comparison of the modeling system with the real system for system exergy efficiency.

To display dynamic behaviour of the model, the variation in system exergy efficiency with environmental (ambient) temperature is shown in Figure 6. As it can be seen from Figure 6, while environmental temperature increases, the exergy efficiency of the system falls. In conclusion, in the general literature, all studies and all engineers, operators and workers researching air-cooled organic Rankine cycles acknowledge that the beneficial exergy of the system is affected by environmental temperature and is known that system exergy efficiency decreases [56–59].

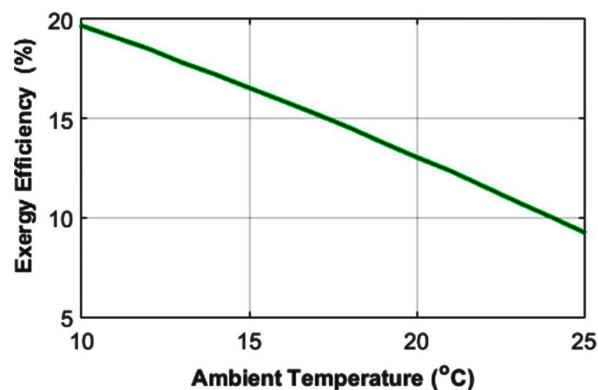


**Figure 6.** The change of exergy efficiency of the modelled system with ambient temperature.

After the modelling of the system mentioned above, the thermodynamic performance of the model for the Sinem GPP with real air-cooled geothermal binary organic Rankine cycle has been maximized with the ABC optimization method. To apply the ABC method to the developed model and thus find the best performance of the Sinem GPP, the main parameters presented in Table 2 are used.

**Table 2.** Main parameters and their values used in the ABC optimization.

Parameters	$1 \leq n \leq 5$	$6 \leq n \leq 10$
Number of colony size (NP)	10	20
Number of food sources	10	20
Number of cycles (stopping criteria)	50	100
Limit	100	100
Number of optimization parameter (D)	1	1

By optimizing the model as maximum exergy efficiency, the optimum values of the pressure, temperature and flow rate data given in Table 2 for the line numbers of Figure 1 are found. During the ABC optimization process, the variable parameters and constraints given in Table 3 are used. The constraints are variable parameters simultaneously. As the real system was modelled according to temperature data at the line numbers in Figure 1, the exergy efficiency of the developed model was not significantly affected by the changes of temperature data. Each temperature change on the system line numbers, especially changes in the source/well temperature and pressure data in the cycle, completely change the model and sometimes result in insolvability. So temperature and pressure data of the real system were accepted as being dependent or kept fixed some places. Because of this reason, all the data except temperature are used for optimization. Thus, some cases are created by grouping the variable/constraint parameters (see Table 3). To maximize the exergy efficiency of the model of the Sinem GPP, the cases accepted for optimizing the model in the best way is listed in the last column of Table 3. Here, the integers specify 12 cases (variable parameter groups). Each of these groups is called as “case”. For example, seeing on the first line of Table 3 indicates that the variable parameter  $P_1$  is included in case 1, case 3 and case 6. To reveal these cases, numerous calculations have been repeated. In conclusion, to evaluate the effects of variable parameters given in Table 3 on exergy efficiencies of the modelling components of the GPP components, 12 cases were determined as optimization conditions.

**Table 3.** The conditions used for the system optimization.

Variable Parameters	Real Values	Constraint Range	Cases Arising from the Grouping of Variable Parameters	
$P_1$	kPa	1040	950–1150	1, 3, 6
$P_{1,steam}$	kPa	1040	950–1150	1, 3, 7, 11
$P_{13}$	kPa	150	115–185	2, 4
$P_{20}$	kPa	119	90–150	2, 5, 11
$\Delta P_{VAP 1}$	kPa	310	0–440	1, 3, 6, 7
$\Delta P_{VAP 2}$	kPa	40	0–230	1, 3, 6, 7, 11
$\Delta P_{PREHE 1}$	kPa	100	0–200	1, 3, 6
$\Delta P_{PREHE 2}$	kPa	120	0–200	1, 3, 7
$\dot{m}_1$	kg/s	445	442–446	1, 6, 11
$\dot{m}_{1,steam}$	kg/s	8.33	8–10	1, 7, 11
$\dot{m}_{12}$	kg/s	160	159.6–161.6	2, 4, 12
$\dot{m}_{19}$	kg/s	169	167–172	2, 5, 12
NCG	%	30	20–40	1, 7, 11
$\dot{m}_a$	kg/s	2000	1600–2400	8, 9, 11, 12
$\dot{m}_c$	kg/s	2000	1600–2400	8, 10, 12
Number of Fan 1	unit	33	21–45	8, 9, 12
Number of Fan 2	unit	36	21–45	8, 10, 12

The behaviour of the optimization process for maximizing the exergy efficiency of the model of the Sinem GPP is illustrated in Figure 7, as a change of exergy efficiency versus cycle number.

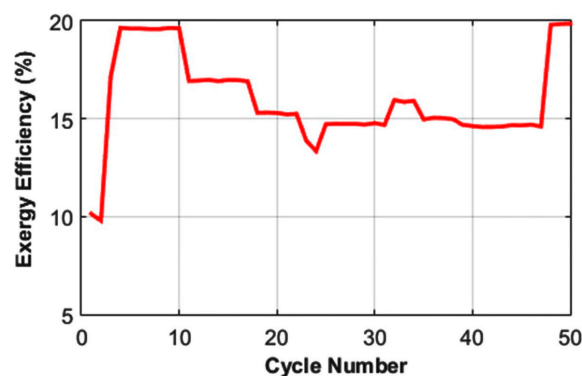


**Figure 7.** The change of exergy efficiency with cycle number during the optimization.

Regarding Figure 7, the system exergy efficiency is taken as the objective function and the function has been maximized. As observed from the figure, although the ABC method may not select a suitable random solution (10.16%) at the initializing stage of finding the best exergy efficiency, it however can rapidly converge to the optimum (19.76% as maximum) exergy efficiency in 4th cycle. It remains at this value until 10th cycle. There are declines in exergy efficiency between 10th and 48th cycles due to random change in the constraint range of variable parameters. Still they are above the real value (14.52%). After 48th cycle, the exergy efficiency has again reached its maximum value. As a result, the ABC optimization process is completed on the model of the GPP.

The variation in system exergy efficiency for 12 cases as optimization conditions of the ABC optimization process is shown in Figure 8. Here Case 0 is the exergy efficiency of the real operating system. Its value is 14.52%. As observed on the figure, for all optimization conditions, their exergy efficiencies are higher than that of Case 0. The exergy efficiency (14.59%) obtained in Case 5 is the closest to that of the real system. This is followed by Cases 7 and 9. Cases 5 and 7 are related to optimization of the pressure of the geofluid along the lines shown in Figure 1 while Case 9 is related to that of TURB 1-related parameters. Especially in the system, Case 12 has the highest value at exergy efficiency as 23.92%. Case 8 as 22.82%, Case 10 as 20.52% and Case 9 as 20.51% come later. In Cases 8, 9, 10 and 12, it is optimized for the condensers-related parameters in the GPP. According to exergy analysis, the highest exergy destruction rate occurred in condenser CON 2. This was followed by VAP 2, CON 1 and the fans. It is observed that, these optimization results show similar results with those of the exergy analysis.

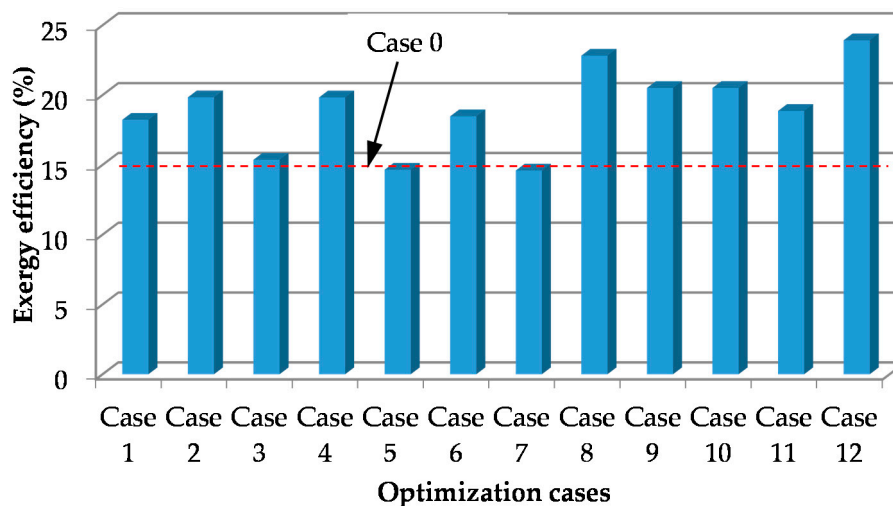
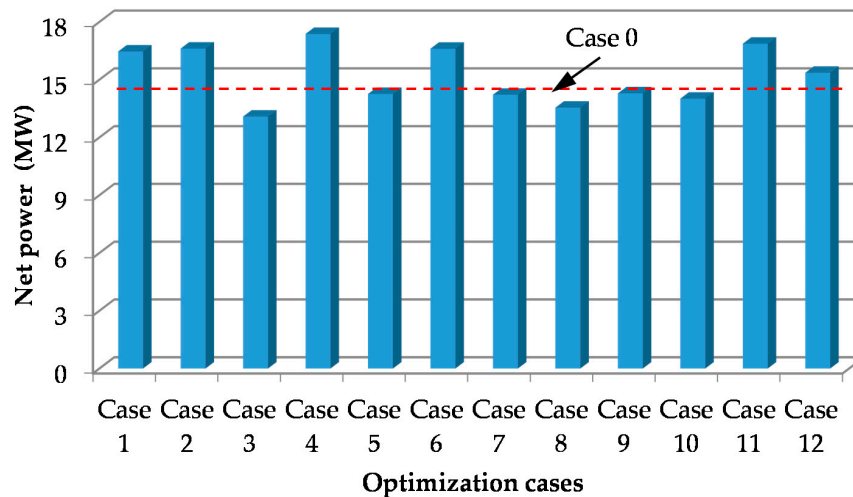


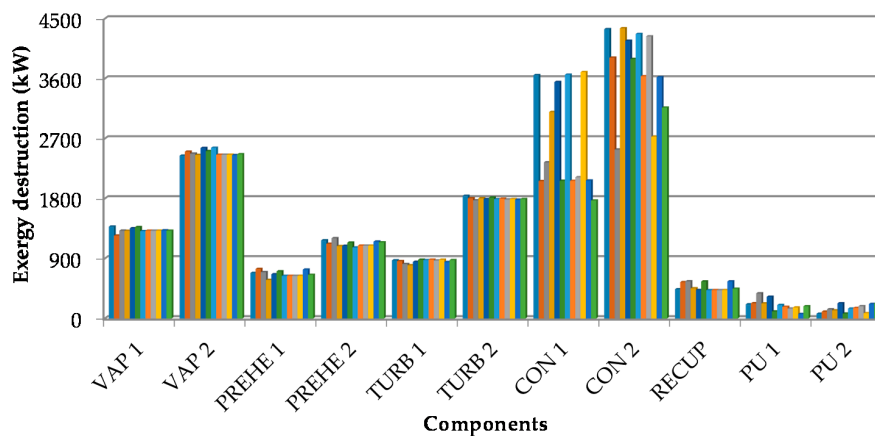
Figure 8. The change of system exergy efficiency according to optimization conditions.

Figure 9 shows the variation in net power generated from the model according to optimization conditions. In the figure, Case 0 states the net power of the real system and its value is 14.21 MW. As seen in the figure, at the end of the optimization process, Cases 3, 8, 9 and 10 have a net power below the value of the real system. When optimized it for n-pentane line-related parameters of TURB 1 (Case 3) and condensers-related parameters (Cases 8–10), they have no much effect on maximum system exergy efficiency. Contrary to the previous conditions, Case 4 with TURB 2-related parameters and Cases 11 and 12 with condensers-related parameters have the highest net power values. The net power rate of Case 4 is 16% larger than that of Case 0. The value is equivalent roughly to 3 MW more electricity generation. For Cases 11 and 12 with condensers-related parameters, this is 15.8% and 14%, respectively. Here it may be concluded that the most important components requiring care during design and operation processes of the Sinem GPP are turbines and condensers. With the aim of maximizing exergy efficiency of the GPP system, the exergy destruction rates occurring from the components for optimization conditions (Cases 1–12) are illustrated in Figure 10. Looking at Figure 10,

under all optimization conditions large fluctuations occur in the amounts of exergy destruction in the condensers. It can be reached that optimization conditions mainly affect condensers. Thus, in the real system the condensers have primary importance and require emergency improvement. Additionally, the result of optimization processes is showed that exergy destruction in condensers can be reduced due to their fluctuations.



**Figure 9.** The change of system net power production according to optimization conditions.



**Figure 10.** According to the optimization conditions (Cases 1–12), the amount of exergy destruction that can occur in the components of the Sinem GPP to ensure maximum exergy efficiency in the system.

Figure 11 shows the exergy destruction rates of the system components for Case 0 (the real system) and Case 4 with TURB 2-related parameters as optimization conditions. It can be observed from Figure 11 that the exergy destruction rates for CON 1 and CON 2 in the real system are 3.65 MW and 4.34 MW while in the ABC optimization process, their values fall to 1.77 MW and 3.16 MW, respectively. In this way contrary to increased exergy destruction rate from pumps, recuperator and pre-heaters, there is a 44% and 41% improvement in the condensers (CON 1 and CON 2), respectively. Of the evaporators, VAP 2 causes more exergy destruction compared to VAP 1 on level I. It can be considered that the steep fall in temperature of the geofluid emerging from VAP 1 causes this situation. Again, in the GPP, the mass flow rate of the geofluid steam added to VAP 2 on level II is not sufficient.

A comparison of exergy destruction rates of the system components for Case 0 and Case 12 as optimization conditions is presented in Figure 12. The results of this graphic are in accordance with the results of Figure 11. In Case 12 there is a reduction of 51.5% and 27% in exergy destruction rates

of condensers CON 1 and CON 2. Due to the pump and recuperator on level I, the percentage fall in level I is greater than that in level II. In this case, PU 1 and PU 2 may be more affected by pressure falls due to pollution and blunting of CON 1 and CON 2.

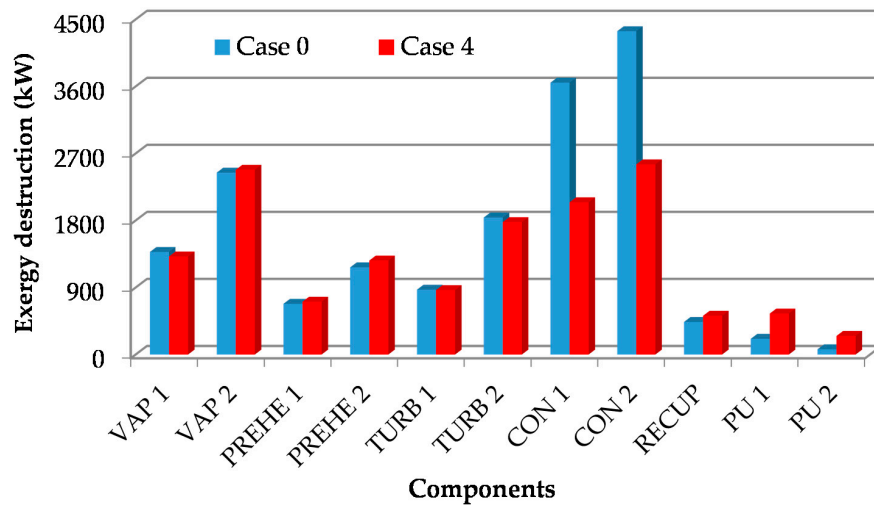


**Figure 11.** Comparison of the exergy destruction rates of the system components at Case 0 for real system and Case 4 of optimization conditions.

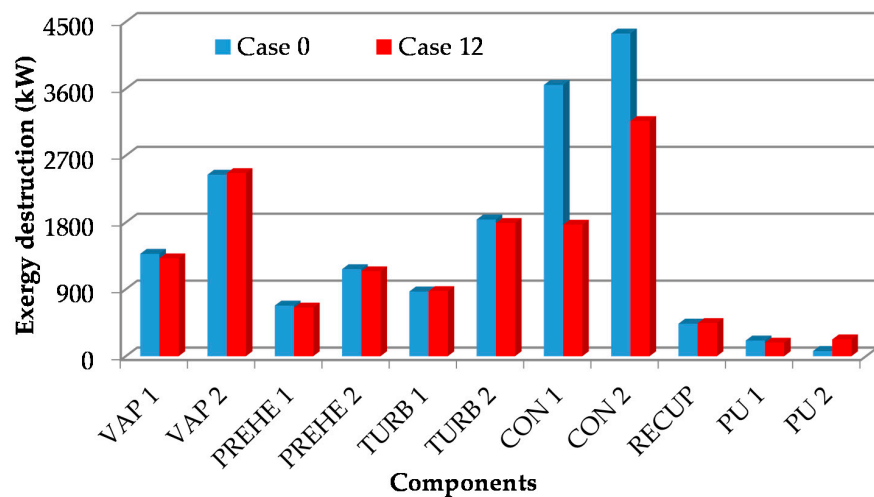


**Figure 12.** Comparison of the exergy destruction rates of the system components at Case 0 for real system and Case 12 of optimization conditions.

The exergy efficiencies of components in the Sinem GPP for all the optimization conditions (Cases 1–12) is given in Figure 13. From Figure 13, under all optimization conditions, the exergy efficiencies especially for the turbines TURB 1 and TURB 2 are similar because the isentropic efficiencies of the turbines were fixed. Thus the power generated from the plant remains constant. In this study the net power of the system has been taken into account as a useful exergy of the system. So this is assessed by subtracting the amount of electricity used to run fans and pumps in the condensers from the generated electricity. As can be seen in Figure 13, the components with highest exergy efficiency are TURB 1 as 93%, VAP 1 as 92% and CON 1 as change in 74–94%. In addition, the exergy efficiency of TURB 2 is 83%. The exergy efficiencies obtained for the turbines are the same as those obtained in the real system. The component with lowest exergy efficiency is the recuperator RECUP with 52%, and 36–54% for the pump PU 1. In TURB 1 and TURB 2, the exergy destruction rate may reach the values in this level due to temperature differences, leaks and pressure falls.

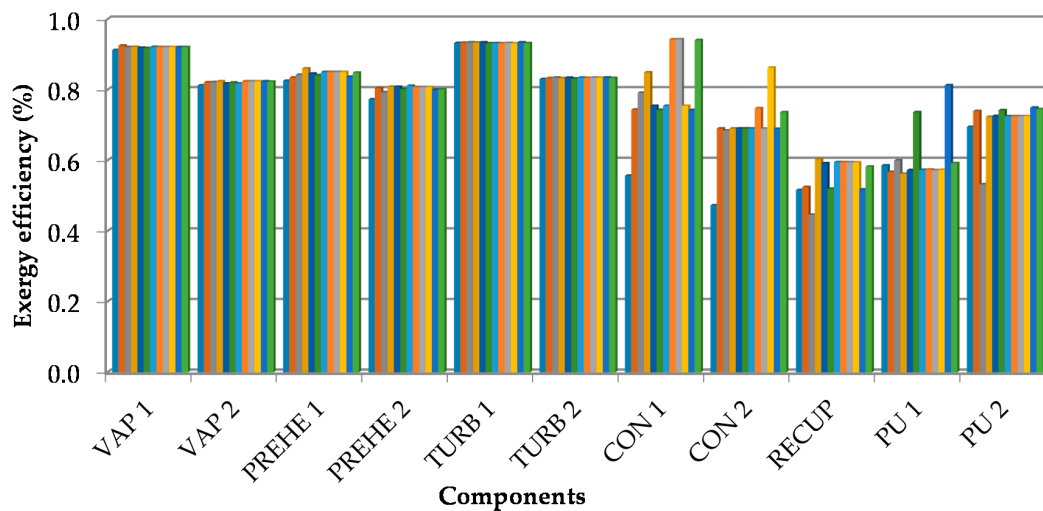


**Figure 13.** According to the optimization conditions (Cases 1–12), the exergy efficiencies that can occur in the components of the Sinem GPP to ensure maximum exergy efficiency in the system.

Under Case 4 and Case 12 as optimization conditions, the exergy efficiencies of system components are compared with the exergy efficiency of the real system components, which can be illustrated in Figures 14 and 15, respectively. In both figures, the exergy efficiencies of TURB 1 and TURB 2 appear to be the same under real and optimization conditions. Regarding Figure 14, in Case 4 with TURB 2-related parameters the exergy efficiencies of the pumps reduces, while increasing those of the condensers. Here it can be said that the exergy destructions of the pumps has increased in Case 4. As a result, the *n*-pentane output from the turbines at high pressure affects the pumps. In real situations, the desire is that turbine output pressure is very low. In conclusion, an increase in the exergy destruction rates from TURB 2 and PU 2 (thus the fall in exergy efficiencies of the pumps) ensures large exergy efficiencies in the condensers. Hence, the generator works efficiently. In Figure 15, Case 12 with condensers-related parameters appears to increase the exergy efficiencies for all GPP components. The exergy efficiencies of the condensers CON 1 and CON 2 increase more than those for other components. Apart from the turbines, exergy efficiencies for all the components increases. As a result, this figure shows how effective the condensers are on the thermodynamic performance of GPPs.

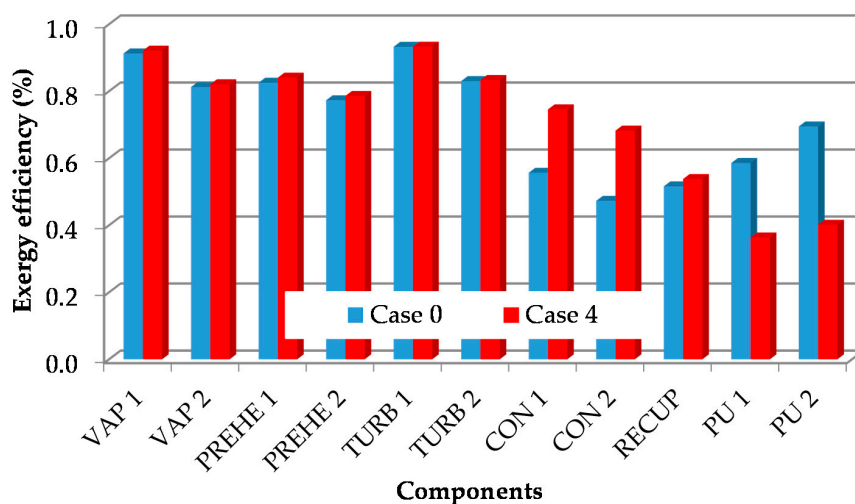


**Figure 14.** Comparison of the exergy efficiencies of the system components at Case 0 for real system and Case 4 of optimization conditions.

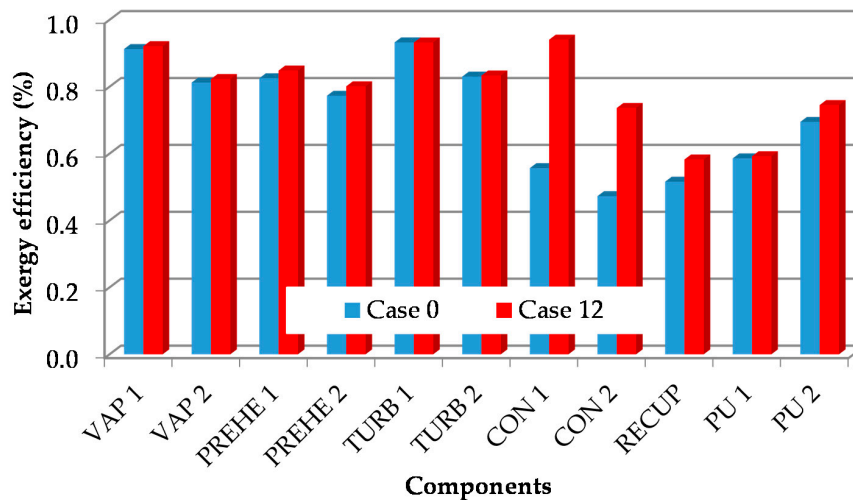


**Figure 15.** Comparison of the exergy efficiencies of the system components at Case 0 for real system and Case 12 of optimization conditions.

With the ABC optimization process, the best thermodynamic performance for Sinem GPP was obtained for optimization conditions in Case 4 and Case 12. Taking note of the total exergy destruction rate for the system under both optimization conditions, the improvement potentials of the system components are presented in Figure 16. On the figure the improvement potential of the GPP appears to be high at 84%. When the study is examined from a different angle, the improvement priority of components may be determined based on the exergy development potential on the general performance. From this figure, the following interpretation may be made; the greatest improvement potential for system components may be obtained from CON 2, VAP 2, CON 1 and TURB 2. It can be understood from Figure 16 that, there is 21.2% improvement potential for CON 2 if a GPP is operated according to Case 12 with condensers-related parameters. According to Case 4, the improvement potentials for CON 2 and VAP 2 are close to each other and nearly 15%. The components with least improvement potential are the pumps (PU 1 and PU 2) and the recuperator (RECUP).

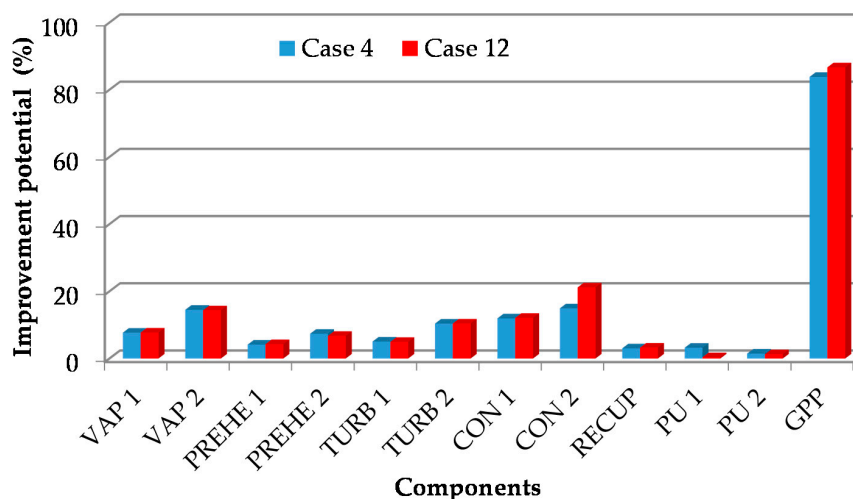


**Figure 16.** Improvement potentials of components according to the total amount of exergy destruction of all the components of the actual GPP.

In Figure 17, the input exergy rate of the real system is noted and the improvement potentials of the system components is compared according to optimization conditions. It can be observed that the

improvement potentials of the components appear to be similar to Figure 16. Wherein the differences are only in the improvement potential percentages and the improvement potential for the exergy input of the whole GPP. On Figure 16, there is a slight difference in the improvement potential in Case 4 and Case 12, while on Figure 17 they are the same. According to the exergy rate entering the system, the improvement potentials for the system components as CON 2, VAP 2, CON 1 and TURB 2 are 1.36%, 0.93%, 0.78% and 0.67%, respectively. However, as stated in the exergy analysis, improvement priority for pumps and fans does not appear in the results of the ABC optimization process.

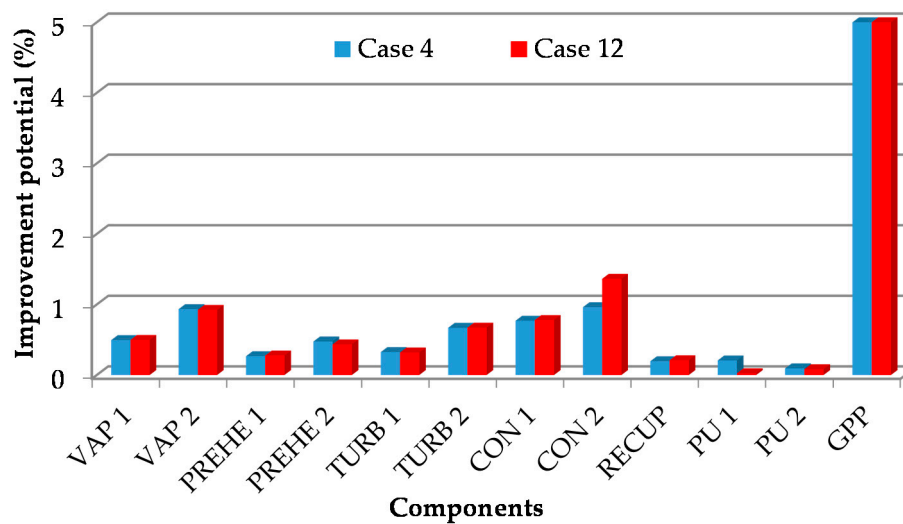


Figure 17. Improvement potentials of the components according to exergy input of the actual system.

#### 4. Discussion and Conclusions

In this study, information is obtained about modelling and performance improvement of the geothermal binary geothermal power plant (GPP) with air-cooled organic Rankine cycle (ORC). As a case study, the exergy analysis according to the Second Law of Thermodynamics is applied to the Sinem GPP, operating currently and belonging to Maren Maraş Electricity Generation Inc. with data collected from the system under operating conditions. Meanwhile, a model is developed to simulate fully and accurately the GPP in terms of thermodynamics. Using the artificial bee colony (ABC) method, the developed model is optimized for thermodynamic performance. With the ABC method, 12 cases are chosen for optimization conditions. Thus, the performance of the power plant can be predicted with reasonable accuracy and at the same time, the physical process to be used to improve the performance of the power plant can be better understood.

Firstly, exergy analysis is performed for the GPP. The largest exergy losses from the power plant occur during re-injection of the geofluid, and then from the condenser, evaporator and pumps. Of the total 53.8 MW exergy input rate into the system, 23.7% is spent for re-injection, 0.5% for release of NCG into nature and 75.8% is exergy rate destroyed by the components of the GPP. According to exergy analysis, the total exergy production of the GPP is 21 MW and the exergy efficiency is 54.52%, after removing parasitic loads. The results of exergy analysis shown that the highest exergy destruction rate occurs in the condensers. The components with the highest exergy destruction rate are ranked as CON 2, VAP 2, CON 1, PU 1, PU 2 and separators. Their percentages are 4.6%, 4.6%, 3.7%, 3.6% and 3.6%, of the total exergy input rate, respectively. This order also determines the components requiring priority improvement.

In this study, a mathematical model fully simulating Sinem GPP accurately and thermodynamically is developed. This model is completed with the MATLAB program, which can rapidly incorporate thermodynamic flow properties from the COOLPROP program. The model uses an iterative method while attempting to estimate the outputs corresponding to component inputs

in the system. This model is used to estimate the true potential of improvement or interactions between components. Fixed values in the model are changed in an attempt to make the model adapt to new conditions. Thus, the model gains dynamism. This model can adapt to environmental temperature and variations in temperature, pressure and flow parameters in all line numbers in the system. However, variations in temperature parameters strongly affect the ORC cycle, it may lead to insolvability. Variable selection and optimization intervals (upper and lower limits) are determined to maximize exergy efficiency of the Sinem GPP with the ABC optimization method. Thus, 12 cases are created with the optimization conditions (Cases 1–12). These cases all maximized exergy efficiency at the GPP. However, the best performance is obtained from Case 4 relating to the 2 turbines and Case 12 relating to the condensers. Case 7 simulates the real system exactly.

As the real Sinem GPP is designed in accordance with parameters relating to geofluid, exergy efficiency of the geothermal brine line did not cause much effect. As the output pressure of the turbines used to produce electricity increased, the condensers began to experience problems (and as a result the fans) and changes in the number of fans ensuring ORC affected the net electrical power generated. The net power generated in Case 4 is 16% larger than that of the real system. This increase is equivalent to electricity production of more than 3 MW. In Case 12 relating to condensers, this value is 14%. Thus, the most important components requiring care in the design and operation of Sinem GPP are turbines and condensers.

The ABC optimization process shows how exergy destruction in all components including condensers can be reduced. For example, the exergy destruction of CON 1 and CON 2 in the real system are 3.65 MW and 4.34 MW, while in the ABC optimization process, these values reduce to 1.77 MW and 3.16 MW, respectively. PU 1 and PU 2 are most affected by pollution and blunting problems in CON 1 and CON 2. Under all optimization conditions, the exergy efficiencies of the turbines TURB 1 and TURB 2 are the same. As a result, for beneficial exergy of the GPP, net power generation is noted. The components with highest exergy efficiency are CON 1 with 94%, TURB 1 with 93% and VAP 1 with 92%. The exergy destruction rates reach this level in TURB 1 and TURB 2 due to temperature differences, leaks and pressure falls.

The improvement potential for Sinem GPP is found to be 84%. Thus greatest improvement among system components are present for CON 2, VAP 2, CON 1 and TURB 2. Components with the least improvement potential are pumps (PU 1 and PU 2) and the recuperator RECUP. According to the exergy rate entering the system, the exergy improvement potentials of system components are in the order CON 2, VAP 2, CON 1 and TURB 2; however this order is not the same in the exergy analysis.

It appears that with developing technology, the efficiency of geothermal power plants continue to increase. At Sinem GPP there are problems such as inability to set the flow rate, temperature and pressure of the geofluid (brine) and/or keeping it low, the high temperature of geofluid, the high working temperature, the use of a recuperator on level I but not on level II, the binary turbines linked to the generator with the same shaft, the insufficient flow of geofluid steam and the high NCG content, the turbine leaks and losses, and the design/operating problems with the air-cooled condenser. Thus, though the exergy inputs are high, the electricity generation amount and efficiency of the power plant are low, so it appears not to work efficiently.

Finally, the ABC optimization method in this study can provide higher quality information than exergy analysis. If geothermal power plants can be studied with similar methods in this study, serious energy and cost savings may be ensured. The ABC optimization method can be completed for all power plants operating in accordance with the organic Rankine cycle.

**Acknowledgments:** The authors gratefully acknowledge the support provided for the present work by the Maren Geothermal Inc. and the personal support of the managing director, Ertan Türk. The authors are very grateful to the reviewers due their appropriate and constructive suggestions as well as their proposed corrections, which have been utilized in improving the quality of the paper.

**Author Contributions:** All authors contributed to writing the article on equal terms. All authors read and approved the final manuscript.

**Conflicts of Interest:** The authors declare no conflict of interest.

## Nomenclature

$c_p$	specific heat ( $\text{kJ}\cdot\text{kg}^{-1}\cdot\text{K}^{-1}$ )
$C$	heat capacity rate ( $\text{kW}\cdot\text{K}^{-1}$ )
$\dot{E}_x$	exergy rate ( $\text{kJ}\cdot\text{s}^{-1}$ or kW)
$h$	specific enthalpy ( $\text{kJ}\cdot\text{kg}^{-1}$ )
$\dot{I}$	irreversibility (exergy destruction) rate (kW)
$\dot{m}$	mass flow rate ( $\text{kg}\cdot\text{s}^{-1}$ )
$P$	pressure (kPa)
$q$	unit heat transfer rate ( $\text{kW}\cdot\text{kg}^{-1}$ )
$\dot{Q}_k$	heat transfer rate (kW)
$s$	specific entropy ( $\text{kJ}\cdot\text{kg}^{-1}\cdot\text{K}^{-1}$ )
$\dot{S}$	entropy rate ( $\text{kJ}\cdot\text{K}^{-1}$ )
$T$	temperature ( $^{\circ}\text{C}$ or K)
$\dot{W}$	work rate, power (kW)

## Greek Symbols

$\Delta$	difference (-)
$\varepsilon$	exergy or second law efficiency (%)
$\tilde{\varepsilon}_k$	effectiveness (-)
$\eta$	energy or first law efficiency (%)
$\Phi$	random number (-)
$\psi$	flow exergy ( $\text{kJ}\cdot\text{kg}^{-1}$ )

## Subscripts

D	destruction
F	fuel
gen	generation
in	input
is	isentropic
j	successive number of elements
k	location
L	loss
out	output
P	product
sys	system
0	reference state

## Appendix A

**Table A1.** The exergy balance equations used for the thermodynamic analysis of the system components.

Component	Exergy Balance	Exergy Efficiency
Vaporizer 1 (VAP 1)	$\dot{E}_{D,VAP1} = (\dot{E}_{x1} - \dot{E}_{x2}) - (\dot{E}_{x12} - \dot{E}_{x11})$	$\varepsilon_{VAP1} = \frac{\dot{E}_{x12} - \dot{E}_{x11}}{\dot{E}_{x1} - \dot{E}_{x2}}$
Vaporizer 2 (VAP 2)	$\dot{E}_{D,PREHE1} = (\dot{E}_{x4} - \dot{E}_{x6}) - (\dot{E}_{x11} - \dot{E}_{x17})$	$\varepsilon_{VAP2} = \frac{\dot{E}_{x19} - \dot{E}_{x18}}{\dot{E}_{x2} - \dot{E}_{x3} + \dot{E}_{x1}' - \dot{E}_{x10} + \dot{E}_{x9}}$
Preheater 1 (PREHE 1)	$\dot{E}_{D,PREHE1} = (\dot{E}_{x4} - \dot{E}_{x6}) - (\dot{E}_{x11} - \dot{E}_{x17})$	$\varepsilon_{PREHE1} = \frac{\dot{E}_{x11} - \dot{E}_{x17}}{\dot{E}_{x4} - \dot{E}_{x6}}$

Table A1. Cont.

Component	Exergy Balance	Exergy Efficiency
Preheater 2 (PREHE 2)	$\dot{E}_{D,PREHE2} = (\dot{E}_{x5} - \dot{E}_{x7}) - (\dot{E}_{x18} - \dot{E}_{x22})$	$\epsilon_{PREHE2} = \frac{\dot{E}_{x18} - \dot{E}_{x22}}{\dot{E}_{x5} - \dot{E}_{x7}}$
Recuperator (RECUP)	$\dot{E}_{D,RECUP} = (\dot{E}_{x17} - \dot{E}_{x16}) - (\dot{E}_{x13} - \dot{E}_{x14})$	$\epsilon_{RECUP} = \frac{\dot{E}_{x13} - \dot{E}_{x14}}{\dot{E}_{x17} - \dot{E}_{x16}}$
Turbine 1 (TURB 1)	$\dot{E}_{D,TURB1} = (\dot{E}_{x12} - \dot{E}_{x13}) - \dot{W}_{TURB1}$	$\epsilon_{TURB1} = \frac{\dot{W}_{TURB1}}{\dot{E}_{x12} - \dot{E}_{x13}}$
Turbine 2 (TURB 2)	$\dot{E}_{D,TURB2} = (\dot{E}_{x19} - \dot{E}_{x20}) - \dot{W}_{TURB2}$	$\epsilon_{TURB2} = \frac{\dot{W}_{TURB2}}{\dot{E}_{x19} - \dot{E}_{x20}}$
Condenser 1 (CON 1)	$\dot{E}_{D,CON1} = (\dot{E}_{x14} - \dot{E}_{x15}) - (\dot{E}_{xb} - \dot{E}_{xa})$	$\epsilon_{CON1} = \frac{\dot{E}_{x14} - \dot{E}_{x15}}{\dot{E}_{xb} - \dot{E}_{xa}}$
For fans (FAN 1)	$\dot{E}_{D,FAN1} = \dot{W}_{FAN1} - (\dot{E}_{xb} - \dot{E}_{xa})$	$\epsilon_{FAN1} = \frac{\dot{E}_{xb} - \dot{E}_{xa}}{\dot{W}_{FAN1}}$
Condenser 2 (CON 2)	$\dot{E}_{D,CON2} = (\dot{E}_{x20} - \dot{E}_{x21}) - (\dot{E}_{xd} - \dot{E}_{xc})$	$\epsilon_{CON2} = \frac{\dot{E}_{x20} - \dot{E}_{x21}}{\dot{E}_{xd} - \dot{E}_{xc}}$
For fans (FAN 2)	$\dot{E}_{D,FAN2} = \dot{W}_{FAN2} - (\dot{E}_{xd} - \dot{E}_{xc})$	$\epsilon_{FAN2} = \frac{\dot{E}_{xd} - \dot{E}_{xc}}{\dot{W}_{FAN2}}$
Pump 1 (PU 1)	$\dot{E}_{D,PU1} = \dot{W}_{PU1} - (\dot{E}_{x16} - \dot{E}_{x15})$	$\epsilon_{PU1} = \frac{\dot{E}_{x16} - \dot{E}_{x15}}{\dot{W}_{PU1}}$
Pump 2 (PU 2)	$\dot{E}_{D,PU2} = \dot{W}_{PU2} - (\dot{E}_{x22} - \dot{E}_{x21})$	$\epsilon_{PU2} = \frac{\dot{E}_{x22} - \dot{E}_{x21}}{\dot{W}_{PU2}}$

Table A2. The balance equations and their restrictions used for the dynamic modelling of the system components.

Component	Modelling Balance	Restrictions
Vaporizer 1 (VAP 1)	$C_1 = \dot{m}_1 c_{p,1}$ $C_{11} = \dot{m}_1 c_{p,11}$ $C_{\min,VAP1} = \min(C_1, C_{11})$ $\dot{Q}_{VAP1,heating} =$ $\tilde{\epsilon}_{VAP1} C_{\min,VAP1} (T_{VAP1,pinch} - T_{11})$ $T_2 = T_{VAP1,pinch} - \frac{\dot{Q}_{VAP1,heating}}{C_1}$ $T_{12} = T_{11} + \frac{\dot{Q}_{VAP1,heating}}{C_{11}}$ $\Delta T_{pinch} = T_{VAP1,pinch} - T_{12}$ $\tilde{\epsilon}_k = q_{real,k} / q_{max,k}$ $\dot{Q}_{VAP1,boiling} = \dot{m}_1 (h_{12g} - h_{12f})$ $= C_1 (T_1 - T_{VAP1,pinch})$	$P_2 = P_1 - \Delta P_{VAP1}$ $P_{11} = P_{12} = P_{16} = P_{17}$
Vaporizer 2 (VAP 2)	$C_{1'} = \dot{m}_{1'} c_{p,1'}$ $C_{18} = \dot{m}_{18} c_{p,18}$ $C_{\min,VAP2} = \min(C_{1'}, C_{18})$ $\dot{Q}_{VAP2,heating} = \tilde{\epsilon}_{VAP2} C_{\min,VAP2} (T_{1'} - T_{18})$ $T_{10} = T_{1'} - \frac{\dot{Q}_{VAP2,heating}}{C_{1'}}$ $T_{19} = T_{18} + \frac{\dot{Q}_{VAP2,heating}}{C_{18}}$ $\dot{Q}_{VAP2,boiling} = \dot{m}_{19} (h_{19g} - h_{19f})$ $= C_2 (T_2 - T_3)$ $\Delta T_{pinch} = T_3 - T_{19}$	$P_3 = P_2 - \Delta P_{VAP2}$ $P_{18} = P_{19} = P_{22}$

Table A2. Cont.

Component	Modelling Balance	Restrictions
Preheater 1 (PREHE 1)	$C_4 = \dot{m}_4 c_{p,4}$ $C_{17} = \dot{m}_{17} c_{p,17}$ $C_{\min,PREHE1} = \min(C_4, C_{17})$ $Q_{PREHE1} = \tilde{\epsilon}_{PREHE1} C_{\min,PREHE1} (T_4 - T_{17})$ $T_6 = T_4 - \frac{Q_{PREHE1}}{C_4}$ $T_{11} = T_{17} + \frac{Q_{PREHE1}}{C_{17}}$	$P_4 = P_6 - \Delta p_{PREHE1}$ $P_{11} = P_{12} = P_{16} = P_{17}$
Preheater 2 (PREHE 2)	$C_5 = \dot{m}_5 c_{p,5}$ $C_{22} = \dot{m}_{22} c_{p,22}$ $C_{\min,PREHE2} = \min(C_5, C_{22})$ $Q_{PREHE2} = \tilde{\epsilon}_{PREHE2} C_{\min,PREHE2} (T_5 - T_{22})$ $T_7 = T_5 - \frac{Q_{PREHE2}}{C_5}$ $T_{18} = T_{22} + \frac{Q_{PREHE2}}{C_{22}}$	$P_5 = P_7 - \Delta p_{PREHE2}$ $P_{18} = P_{19} = P_{22}$
Recuperator (RECUP)	$C_{13} = \dot{m}_{13} c_{p,13}$ $C_{16} = \dot{m}_{16} c_{p,16}$ $C_{\min,RECUP} = \min(C_{13}, C_{16})$ $\dot{Q}_{RECUP} = \tilde{\epsilon}_{RECUP} C_{\min,RECUP} (T_{13} - T_{16})$ $T_{14} = T_{13} - \frac{\dot{Q}_{RECUP}}{C_{13}}$ $T_{17} = T_{16} + \frac{\dot{Q}_{RECUP}}{C_{16}}$	$P_{13} = P_{14} = P_{15}$ $P_{11} = P_{16} = P_{17}$
Condenser 1 (CON 1)	$C_a = \dot{m}_a c_{p,a}$ $C_{14} = \dot{m}_{14} c_{p,14}$ $C_{\min,CON1} = \min(C_a, C_{14})$ $Q_{CON1,cooling} = \tilde{\epsilon}_{CON1} C_{\min,CON1} (T_{14} - T_a)$ $T_{15} = T_{14} - \frac{Q_{CON1,cooling}}{C_{14}}$ $T_b = T_a + \frac{Q_{CON1,cooling}}{C_a}$ $\dot{Q}_{CON1,cooling} = \dot{m}_{15} (h_{15g} - h_{15f})$ $\quad = C_a (T_{b,2} - T_a)$	$P_{13} = P_{14} = P_{15}$
Condenser 2 (CON 2)	$C_c = \dot{m}_c c_{p,c}$ $C_{20} = \dot{m}_{20} c_{p,20}$ $C_{\min,CON2} = \min(C_c, C_{20})$ $Q_{CON2,cooling} = \tilde{\epsilon}_{CON2} C_{\min,CON2} (T_{20} - T_c)$ $T_{21} = T_{20} - \frac{Q_{CON2,cooling}}{C_{20}}$ $T_d = T_c + \frac{Q_{CON2,cooling}}{C_c}$ $\dot{Q}_{CON2,cooling} = \dot{m}_{21} (h_{21g} - h_{21f})$ $\quad = C_c (T_{d,2} - T_c)$	$P_{20} = P_{21}$

## References

- Malafeh, S.; Sharp, B. Role of royalties in sustainable geothermal energy development. *Energy Pol.* **2015**, *85*, 235–242. [CrossRef]
- Flovenz, O.G. General aspects of geothermal energy. In *Geo-Survey for the World Bank at Renewable Energy Training Program*; University of Iceland: Reykjavík, Iceland, 2012.
- Schiel, K.; Baume, O.; Caruso, G.; Leopold, U. GIS-based modelling of shallow geothermal energy potential for CO<sub>2</sub> emission mitigation in urban areas. *Renew. Energy* **2016**, *86*, 1023–1036. [CrossRef]
- Lee, K.C. Classification of geothermal resources by exergy. *Geothermics* **2001**, *30*, 431–442. [CrossRef]
- Chamorro, C.R.; Mondejar, M.E.; Ramos, R.; Segovia, J.J.; Martin, M.C.; Villamanan, M.A. World geothermal power production status: Energy, environmental and economic study of high enthalpy technologies. *Energy* **2012**, *42*, 10–18. [CrossRef]

6. Dickson, M.; Fanelli, M. What is geothermal energy? In *Instituto di Geoscienze e Georisorse*; CNR: Pisa, Italy, 2004.
7. Bertani, R. Geothermal power generation in the World 2005–2010 update report. In Proceedings of the World Geothermal Congress, Bali, Indonesia, 25–29 April 2010.
8. General Directorate of Renewable Energy, History of Geothermal Energy. Available online: <http://www.eie.gov.tr> (accessed on 11 January 2017).
9. Erdogmus, B.; Toksoy, M.; Ozerdem, B.; Aksoy, N. Economic assessment of geothermal district heating systems: A case study of Balcova-Narlidere, Turkey. *Energy Build.* **2006**, *38*, 1053–1059. [[CrossRef](#)]
10. Energy Information Administration, Geothermal Power Plants. Available online: <http://www.eia.gov> (accessed on 12 February 2017).
11. Trinnaman, J.; Clarke, A. *2010 Survey of Energy Resources*; World Energy Council: London, UK, 2010.
12. Saleh, B.; Koglbauer, G.; Wendland, M.; Fischer, J. Working fluids for low-temperature organic Rankine cycles. *Energy* **2007**, *32*, 1210–1221. [[CrossRef](#)]
13. Kestin, J.; DiPippo, R.; Khalifa, H.E.; Ryley, D.J. *Source Book on the Production of Electricity from Geothermal Energy*; US Government Printing Office: Washington, DC, USA, 1980.
14. Bruges, E.A. *Available Energy and Second Law Analysis*; Butterworth Scientific Pub.: London, UK, 1959.
15. Rogers, G.; Mayhew, Y. *Engineering Thermodynamics Work and Heat Transfer*; Longman Scientific and Technical: Harlow, Essex, UK, 1993.
16. Ileri, A.; Gurer, T. Energy and exergy utilization in Turkey during 1995. *Energy* **1998**, *23*, 1099–1106. [[CrossRef](#)]
17. Pierobon, L.; Benato, A.; Scolari, E.; Haglind, F.; Stoppato, A. Waste heat recovery technologies for offshore platforms. *Appl. Energy* **2014**, *136*, 228–241. [[CrossRef](#)]
18. Stoppato, A.; Cavazzini, G.; Ardizzon, G.; Rossetti, A. A PSO (particle swarm optimization)-based model for the optimal management of a small PV(Photovoltaic)-pump hydro energy storage in a rural dry area. *Energy* **2014**, *76*, 168–174. [[CrossRef](#)]
19. Cavazzini, G.; Dal Toso, P. Techno-economic feasibility study of the integration of a commercial small-scale ORC in a real case study. *Energy Convers. Manag.* **2015**, *99*, 161–175. [[CrossRef](#)]
20. Benato, A.; Kaern, M.R.; Pierobon, L.; Stoppato, A.; Haglind, F. Analysis of hot spots in boilers of organic Rankine cycle units during transient operation. *Appl. Energy* **2015**, *151*, 119–131. [[CrossRef](#)]
21. Pezzuolo, A.; Benato, A.; Stoppato, A.; Mirandola, A. The ORC-PD: A versatile tool for fluid selection and Organic Rankine Cycle unit design. *Energy* **2016**, *102*, 605–620. [[CrossRef](#)]
22. Benato, A.; Macor, A. Biogas engine waste heat recovery using organic Rankine cycle. *Energies* **2017**, *10*, 327. [[CrossRef](#)]
23. Gurgenci, H. Performance of power plants with organic Rankine cycles under part-load and off-design conditions. *Sol. Wind Technol.* **1986**, *36*, 45–51. [[CrossRef](#)]
24. Sun, J.; Li, W. Operation optimization of an organic Rankine cycle (ORC) heat recovery power plant. *Appl. Therm. Eng.* **2011**, *31*, 2032–2041. [[CrossRef](#)]
25. Calise, F.; Capuozzo, C.; Carotenuto, A.; Vanoli, L. Thermoeconomic analysis and off-design performance of an organic Rankine cycle powered by medium temperature heat sources. *Sol. Energy* **2013**, *103*, 595–609. [[CrossRef](#)]
26. Bamgbopa, M.O.; Uzgoren, E. Numerical analysis of an organic Rankine cycle under steady and variable heat input. *Appl. Energy* **2013**, *107*, 219–228. [[CrossRef](#)]
27. Bamgbopa, M.O.; Uzgoren, E. Quasi-dynamic model for an organic Rankine cycle. *Energy Convers. Manag.* **2013**, *72*, 117–124. [[CrossRef](#)]
28. Manente, G.; Toffolo, A.; Lazzaretto, A.; Paci, M. An organic Rankine cycle off design model for the search of the optimal control strategy. *Energy* **2013**, *58*, 97–106. [[CrossRef](#)]
29. Wang, J.; Yan, Z.; Zhao, P.; Dai, Y. Off-design performance analysis of a solar powered organic Rankine cycle. *Energy Convers. Manag.* **2014**, *80*, 150–157. [[CrossRef](#)]
30. Fu, B.R.; Hsu, S.W.; Lee, Y.R.; Hsieh, J.C.; Chang, C.M.; Liu, C.H. Performance of a 250 kW organic rankine cycle system for off-design heat source conditions. *Energies* **2014**, *7*, 3684–3694. [[CrossRef](#)]
31. Hu, D.; Zheng, Y.; Wu, Y.; Li, S.; Dai, Y. Off-design performance comparison of an organic Rankine cycle under different control strategies. *Appl. Energy* **2015**, *156*, 268–279. [[CrossRef](#)]
32. Yousefzadeha, M.; Uzgoren, E. Mass-conserving dynamic organic Rankine cycle model to investigate the link between mass distribution and system state. *Energy* **2015**, *93*, 1128–1139. [[CrossRef](#)]

33. Ziviani, D.; Woodland, B.J.; Georges, E.; Groll, A.E.; Braun, J.E.; Horton, W.T.; Broek, M.V.D.; Paepe, M.D. Development and a validation of a charge sensitive organic Rankine cycle (ORC) simulation tool. *Energies* **2016**, *9*, 389. [CrossRef]
34. Manente, G.; Lazzaretto, A.; Bonamico, E. Design guidelines for the choice between single and dual pressure layouts in organic Rankine cycle (ORC) systems. *Energy* **2017**, *123*, 413–431. [CrossRef]
35. Dickes, R.; Dumont, O.; Daccord, R.; Quoilin, S.; Lemort, V. Modelling of organic Rankine cycle power systems in off-design conditions: An experimentally-validated comparative study. *Energy* **2017**, *123*, 710–727. [CrossRef]
36. Anderson, J. A vapor turbine geothermal power plant. *Geothermics* **1970**, *2*, 1530–1532. [CrossRef]
37. Bliem, C.; Zangrando, F.; Hassani, V. Value analysis of advanced heat rejection systems for geothermal power plants. In Proceedings of the 31st Intersociety Energy Conversion Engineering Conference, Washington, DC, USA, 11–16 August 1996; pp. 1250–1253.
38. Kanoglu, M. Exergy analysis of a dual-level binary geothermal power plant. *Geothermics* **2002**, *31*, 709–724. [CrossRef]
39. Ozturk, H.K.; Atalay, O.; Yilanci, A.; Hepbasli, A. Energy and exergy analysis of Kizildere geothermal power plant, Turkey. *Energy Sources* **2006**, *28*, 1415–1424. [CrossRef]
40. Hettiarachchi, H.D.M.; Golubovic, M.; Worek, W.M.; Ikegami, Y. Optimum design criteria for an organic Rankine cycle using low-temperature geothermal heat sources. *Energy* **2007**, *32*, 1698–1706. [CrossRef]
41. Sohel, M.I.; Sellier, M.; Brackney, L.J.; Krumdieck, S. Efficiency improvement for geothermal power generation to meet summer peak demand. *Energy Policy* **2009**, *37*, 3370–3376. [CrossRef]
42. Franco, A.; Villani, M. Optimal design of binary cycle power plants for water-dominated, medium-temperature geothermal fields. *Geothermics* **2009**, *38*, 379–391. [CrossRef]
43. Sohel, M.I.; Sellier, M.; Brackney, L.J.; Krumdieck, S. An iterative method for modelling the air-cooled organic Rankine cycle geothermal power plant. *Int. J. Energy Res.* **2011**, *35*, 436–448. [CrossRef]
44. Ghasemi, H.; Paci, M.; Tizzanini, A.; Mitsos, A. Modeling and optimization of a binary geothermal power plant. *Energy* **2013**, *50*, 412–428. [CrossRef]
45. Kipaş Holding, Geothermal Energy. Available online: <http://kipas.com.tr/en-US/portfolio/geothermal-energy> (accessed on 11 January 2017).
46. Tsatsaronis, G. Design optimization using exergoeconomics. In *Thermodynamic Optimization of Complex Energy Systems*; Kluwer Academic Publishers: Dordrecht, The Netherlands, 1999.
47. Bell, I.H.; Quoilin, S.; Wronski, J.; Lemort, V. CoolProp: An open-source reference quality thermophysical property library. In Proceedings of the ASME ORC 2nd International Seminar on ORC Power Systems, Rotterdam, The Netherlands, 7–8 October 2013.
48. Bell, I.H.; Wronski, J.; Quoilin, S.; Lemort, V. Pure and pseudo-pure fluid thermophysical property evaluation and the open-source thermophysical property library coolprop. *Ind. Eng. Chem. Res.* **2014**, *53*, 2498–2508. [CrossRef] [PubMed]
49. MathWorks, Matlab. Available online: <http://www.mathworks.com/products/matlab> (accessed on 15 April 2017).
50. Ozgener, L.; Hepbasli, A.; Dincer, I. A key review on performance improvement aspects of geothermal district heating systems and applications. *Renew. Sustain. Energy Rev.* **2007**, *11*, 1675–1697. [CrossRef]
51. Karaboga, D. *An Ideal Based on Honey Bee Swarm for Numerical Optimization*; Technical Report—TR06; Erciyes University: Kayseri, Turkey, 2005.
52. Karaboga, D.; Akay, B. A comparative study of artificial bee colony algorithm. *Appl. Math. Comput.* **2009**, *214*, 108–132. [CrossRef]
53. Karaboga, D.; Ozturk, C. A novel clustering approach: Artificial Bee Colony (ABC) algorithm. *Appl. Soft Comput.* **2011**, *11*, 652–657. [CrossRef]
54. Karaboga, D.; Basturk, B. A powerful and efficient algorithm for numerical function optimization: Artificial Bee Colony (ABC) algorithm. *J. Glob. Optim.* **2007**, *39*, 459–471. [CrossRef]
55. Karaboga, D.; Basturk, B. Artificial Bee Colony (ABC) optimization algorithm for solving constrained optimization problems. *Found. Fuzzy Log. Soft Comput.* **2007**, *4529*, 789–798.
56. DiPippo, R. The effect of ambient temperature on geothermal binary-plant performance. *Geotherm. Hot Line* **1989**, *19*, 68–70.

57. DiPippo, R. Second Law assessment of binary plants generating power from low-temperature geothermal fluids. *Geothermics* **2004**, *33*, 565–586. [[CrossRef](#)]
58. DiPippo, R. *Geothermal Power Plants: Principles, Applications and Case Studies*; Elsevier Ltd.: Oxford, UK, 2005.
59. DiPippo, R. *Geothermal power plants: Principles, Applications, Case Studies, and Environmental Impact*; Elsevier Ltd.: Oxford, UK, 2008.



© 2017 by the authors. Licensee MDPI, Basel, Switzerland. This article is an open access article distributed under the terms and conditions of the Creative Commons Attribution (CC BY) license (<http://creativecommons.org/licenses/by/4.0/>).